SARS-CoV-2 spike antibodies cross-react with dengue virus and enhance infection *in vitro* and *in vivo*

Kamini Jakhar[1†], Sudipta Sonar[1†], Gagandeep Singh[2], Tejeswara Rao Asuru[3†], Garima Joshi[3†], Nisha Beniwal[1], Tania Sarkar[1], Mahima Tiwari[1], Jaskaran Kaur[1], Deepak Kumar Rathore[4], Banwari Lal[1], Sandeep Kumar[1], Puneet Srivastav[1], Satendra Kumar[1], Vikas Phagna[1], Sushma Mithina[1], Lokesh Kumar[1], Vishal Gupta[1,5], Pallavi Kshetrapal[6], Savita Singh[6], Nitya Wadhwa[6], Ramachandran Thiruvengadam[6], Sreevatsan Raghavan[6], Mudita Gosain[6], Tripti Shrivastava[1], Sankar Bhattacharyya[1], Shailendra Asthana[2], Prasenjit Guchhait[3] and Shailendra Mani[1*]

† Contributed equally

*Corresponding author

Corresponding author: Shailendra Mani, PhD.

Email: shailendramani@thsti.res.in

Author affiliations:

1. Centre for Virus Research, Therapeutics and Vaccines, Translational Health Science and Technology Institute, Faridabad, Haryana, India-120001
2. Computational Biophysics and CADD group, Computational and Mathematical Biology Centre (CMBC), Translational Health Science and Technology Institute (THSTI), Faridabad, Haryana, India-120001
3. Molecular Medicine, Regional Centre for Biotechnology, Faridabad, Haryana, India-120001
4. Centre for Immunobiology and Immunotherapy, Translational Health Science and Technology Institute, Faridabad, Haryana, India-120001

5. Translational Health Science and Technology Institute, Faridabad, Haryana, India-120001
6. Centre for Maternal and Child Health, Translational Health Science and Technology Institute, Faridabad, Haryana, India-120001

Abstract:

The presence of non-neutralizing antibodies of any dengue serotype, increase the severity of subsequent infection by other dengue serotypes. During SARS-CoV-2 pandemic, the number of symptomatic dengue cases increased in India. We describe that antibodies isolated from convalescent plasma from COVID-19 patients enhances DENV2 infection in vitro. CR3022, one antibody against SARS-CoV-2 spike protein, also showed elevated DENV2 infection in vitro. In silico protein-protein interactions between the spike antibodies and the DENV2 E-protein revealed significant interactions. Likewise, few monoclonal/polyclonal antibodies against SARS-CoV-2 showed increased dengue infection in vitro. Importantly, the AG129 mice infected with SARS-CoV-2 three-weeks prior to DENV2 infection, showed elevated dengue pathogenesis. Thus, highlighting the possibilities of elevated infection and symptomatic dengue disease in COVID-19 survivors.

Keywords: SARS-CoV-2; Dengue Virus; Cross-reactivity; Antibody-Dependent Enhancement; AG129 Mice model

Introduction

Dengue is endemic to more than 120 countries with Asia contributing 70% of the global burden (1). Dengue virus (DENV) circulates as four serotypes (DENV 1-4) each containing multiple distinct genotypes. DENV infection can cause mild fever or lead to severe forms like Dengue Haemorrhagic Fever (DHF) and Dengue Shock Syndrome (DSS). Primary infection provides lifelong immunity to homotypic secondary infection but gives partial immunity from heterotypic challenge. Heterotypic secondary infections present with severe symptoms, due to higher viremia catalyzed by Antibody-dependent Enhancement (ADE). Sub-neutralizing antibodies that bind to heterotypic DENV promote FcR-mediated viral entry into cells (2). A stable attachment to Fc receptors by these antibodies, without reaching the neutralization threshold leads to ADE (3).

The dynamics of DENV infections during the SARS-CoV-2 pandemic vary globally. A 16% decline in dengue incidences was reported in 2020-21 compared to pre-COVID-19 (4). However, S. Khan *et. al.* revealed a substantial surge in dengue cases in 2021 in specific South Asian countries, including India (~3-fold), Pakistan (>7-fold), and Bangladesh (>19-fold). This contrasted with a noteworthy decline of about 36% across Southeast Asia and Latin America (5). Several regional, environmental, and pandemic-related elements have been reported to shape these intricate dynamics. Disruptions in routine mosquito vector surveillance and control programs during COVID-19 lockdowns may have led to a rise in dengue cases, highlighting the crucial role of vector control in disease prevention. Similar pathology of DENV and COVID-19 presented diagnostic challenges, potentially contributing to underreporting (4) (6) (7) (8) (9).

Some studies indicate that ADE due to prior SARS-CoV-2 infection may elevate the risk of symptomatic and/or severe dengue. In Pakistan, a significant increase in dengue-related deaths

71 (linked to DENV-2 prevalence) was observed in patients with a pre-exposure to SARS-CoV-2
72 (10).
73 Modest serological cross-reactivity between SARS-CoV-2 and DENV-2 has been reported (11)
74 (12) (13). However, it is unclear if this would have any clinical impact on dengue cases (14). A
75 study reported rabbit IgG against purified SARS-CoV-2 S1-RBD cross-reacts with DENV
76 Envelope (E), precursor-membrane (PrM), and Non-structural protein 1 (NS1). However, these
77 antibodies did not enhance DENV infection in THP-1 cells expressing FcR. Moreover, they
78 impeded DENV infection at high concentrations (15). Another study showed *in vitro* inhibition
79 of dengue infection by sera from convalescent COVID-19 patients' sera (16).
80 Nath *et. al.* demonstrated serological cross-reactivity of SARS-CoV-2 positive serum samples
81 with DENV1 and that the sera neutralized DENV1 (16). Anti-S1-RBD antibodies were shown
82 to impede DENV infection at a specific concentration and COVID-19 patients' sera exhibited a
83 neutralizing ability against dengue infection (15)**.** El-Qushayri *et al.,* in their systematic review,
84 aimed to assess the clinical outcomes of patients with dengue and COVID-19 co-infection. They
85 reported a high mortality rate in co-infected patients (19.1%), significantly exceeding the
86 estimated global mortality rates for dengue (1.3%) and COVID-19 (2.04%). Also, they found
87 that the hospital stay duration for co-infected individuals was longer than the reported median
88 stays for standalone COVID-19 and dengue cases (17). Although, insightful, more information
89 on the stoichiometry of the virus and antibodies in these studies, would have been useful, since
90 it is crucial for understanding antibody-virus interactions and the potential for ADE
91 Here, we evaluated the effect of preexisting SARS-CoV-2 antibodies on DENV-2 infection
92 using cell-based assays and mouse model of DENV infection.
93
94 **Results:**

95 ***In silico* interaction mining drives the cross-recognition of DENV-E protein by anti-**
96 **Spike and anti-RBD SARS-CoV-2 antibodies**
97 To assess the cross-reactivity of SARS-CoV-2 Spike antibodies with DENV-2 E-protein dimer
98 we used an *in silico* approach (Fig. 1A, B). We selected a panel of reported SARS-CoV-2
99 antibodies, based on their structure data (extent of their characterization, availability of the
100 structure information of their co-crystals with low resolution, preferably below 4 A°.) and
101 biological relevance (neutralization potential against SARS-CoV-2, target epitopes, etc.; Table-
102 S1). For the identification of DENV-2 E epitopes, C8 antibody against E-protein dimer (Fab
103 region, PDB-id: 4UTA) was used to characterize the interaction site based on interaction
104 fingerprinting. For identifying the cross-reactive antibodies forming the most promising
105 complexes with the E-protein; selected SARS-CoV-2 antibodies' protein-protein (PP) blind
106 docking was carried out with the whole DENV-2 E dimer. The consensus docked poses
107 obtained from Piper and HDOCK tools were used for post-docking qualitative and quantitative
108 analysis (pose selection and pose-filtering criteria). The top three SARS-CoV-2 antibodies
109 forming the complexes with DENV-2 in terms of docking energy, interaction fingerprinting
110 with co-crystal and MM-GBSA scores are CR3022 (Fab region, PDB-id:6W7Y), S2E12 ab
111 (Fab region, PDB-id:7K45) and DMAb 2196 (Fab region, PDB:8D8R) (Fig. 1C).
112 To quantitate their binding association at the residue level, major contributing amino acids were
113 identified by residue-wise decomposition analysis setting the cut-off value of -1·5 kcal/mol.
114 For the C8 antibody (4UTA) binding with DENV-2 E-protein, the interacting epitopes were
115 majorly localized in Domain II (Fig. 1D). The binding sites of CR3022, S2E12 ab, and DMAb
116 2196 antibodies were found to overlap with C8 binding site (Fig. 1D). The contributing residues
117 for all three antibodies were majorly located in Domain II including Fusion loop (Figure 1E,
118 F). The findings of overlapping residues between C8 and the three SARS-CoV-2 interacting
119 antibodies corroborate well with previously reported study (18). From the interaction analysis,

120 the R73 appeared as the most common interacting residue in all antibodies. The pair-wise
121 interaction analysis confirmed considerable overlapping residues between SARS-CoV-2 and
122 DENV-2 antibodies (Figure 1E and 1F). Key residues that overlap between DENV-2 and at
123 least two antibodies of SARS-CoV-2 are R73 (common among all), T70, S72 (Domain-II), R99
124 and N103 (Fusion loop) and E311 (Domain-III). We also performed the mining of paratope
125 residues of SARS-CoV-2 antibodies with equal and/or increased interaction energy as C8 and
126 identified overlapping residues between C8 and CR3022 (Figure S1).
127 Overall, the interaction maps and per-residue energetic decompositions showed that there were
128 several common residues involved in the interaction of DENV-2-E with C8 and CR3022,
129 S2E12 ab and DMAb 2196 antibodies indicating a high likelihood of cross-reactivity (Figure
130 1G and 1H, Table S2). The paratope residues involved in interaction of E-protein with CR3022
131 were also identified (Table-S3) and their interactions were assessed (Fig. S2).
132
133 **SARS-CoV-2 spike antibody CR3022 cross-reacts with DENV-2 and enhances DENV**
134 **infection *in vitro***
135 Based on the computational outcomes, one of the antibodies, CR3022, which showed the
136 highest affinity with DENV-2 E protein, was studied further. Based on the dengue virus
137 susceptibility and cells monolayer robustness, we selected C6/36 cell line for confocal studies.
138 Confocal microscopy images of CR3022 showed a statistically significant cross-reactivity with
139 an average Mean Fluorescence Intensity (MFI) of 7·68 (p-value<0·0001) (Fig. 2A). Bio-Layer
140 Interferometry (BLI), showed high affinity with a dissociation constant (KD) of <1·0pM with
141 Spike protein (Fig. 2B(i)), and 2·83 μM with DENV-2 E-protein (Fig. 2B(ii)). Further, we
142 observed a significant augmentation in the percentage of DENV-infected K562 cells with
143 CR3022 antibody (p-value=0·01) in comparison to untreated virus control (Fig. 2C).
144

145 **SARS-CoV-2 convalescent plasma enhances DENV infection *in vitro***

146 Samples from convalescent COVID-19 patients (n=48, Table-S4) from different time intervals
147 of the pandemic were tested for their ability to cause ADE. We used FcγR-I, II and III
148 expressing K562 and U937 cell lines. Both cell lines were shown to predominantly express
149 FcγR-II (Fig. S3), as reported previously (19). The basal value of the only virus infection
150 obtained in cell lines are normalized to the tested samples in order to calculate the fold change
151 and graphs are plotted against virus infection (no serum) vs virus infection (incubated with
152 serum) in tested samples. The DENV-2 infected K562 cells were observed to increase from 1
153 to 236 times in the first set of convalescent samples (recovered individuals during Wuhan
154 wave), 77 to 235 times in the second set of convalescent samples (recovered individuals
155 during/around the delta wave), and 44 to 172 times in the third set of convalescent samples
156 (recovered individuals during omicron wave), compared to untreated virus control (Fig. 3A-C).
157 The FACS gating strategy is given in Fig. S4. To confirm that the observed ADE effect was
158 specifically mediated by antibodies present in the serum, IgG was purified from convalescent
159 samples that exhibited high ADE activity. The assay was then performed using 10 µg of purified
160 IgG and DENV-2 (clinical strain INDI-60). A significant enhancement of DENV-2 infection
161 was observed in K562 cells incubated with purified IgGs from the convalescent samples #144
162 ($P < 0.0001$), #150 ($P < 0.0001$), and #151 ($P < 0.0002$), compared to the virus control, (Fig.
163 3D).

164 Using a subset of the convalescent plasma samples (n=15) similar results were observed in
165 U937 cells, where DENV-2 infection was enhanced in the range of 32 to 292 times as compared
166 to the virus control (Fig. S5A-B). A virus neutralization assay with SARS-CoV-2 Wuhan strain
167 (Table-S5), did not show any association between the neutralizing antibody titer and
168 enhancement in Dengue virus infection in convalescent plasma treated samples. (Fig. S6A-D).

169 A representative quantitative PCR assay for intracellular DENV-2 genomic RNA showed a
170 higher viral load in 70% of COVID-19 convalescent plasma treated samples as compared to the
171 control (Fig. S7). This data correlates with the increase in DENV-2 positive cells observed in
172 flow cytometry. Determination of the infectious titer of DENV produced from infected cells by
173 focus-forming unit assay also showed a significant increase in the Foci-forming units/ml
174 (FFU/ml) in COVID-19 convalescent plasma treated samples as compared to control (Fig. S8).
175

176 **SARS-CoV-2 antibodies enhance dengue virus infection *in vivo***

177 To validate the *in silico* and *in vitro* findings, we performed *in vivo* experiments where we took
178 AG129 (Immunocompromised, lack of IFNAR1 and IFNGR1) mice within 6-8 weeks age
179 group (N=21). The mice were divided into three groups, Group 1 as mock (G1, N=5), Group 2
180 as dengue virus control (G2, N=8), and Group 3 as test with both SARS-CoV-2 and dengue
181 virus infection (G3, N=8). G2 was infected with dengue virus infection at day 21 and G3 was
182 infected with SARS-CoV-2 virus at day 0 followed by dengue virus infection at day 21. Both
183 G2 and G3 mice were infected with adeno-ACE-2 (Ad5CMVh, The University of Iowa Viral
184 Vector Core Facility) viral vector at -5 days which is essential for SARS-CoV-2 infection. Body
185 weight was observed for all the animals till day 27 when they were euthanized as shown in the
186 schematic experimental plan (Fig. 4A). Average body weight in G2 mice group decreased at
187 day 3 but it recovered with time (Fig. 4B). A significant decrease of body weight was observed
188 in G3 as compared to G2.

189 We further tested the antibody response against SARS-CoV-2 spike antigen at day 21 before
190 DENV-2 infection, we observed the anti-spike IgG antibody response in all mice in G3 (Fig.
191 4C). Next, the live dengue virus particles determined in serum samples collected on day 27
192 (Fig. 4D), the data revealed a notable increase in number of viral particles in G3 mice group as
193 compared to G2 mice group indicating enhancement of dengue infection with SARS-CoV-2

194 virus. Next, we tested the viral replication in the liver and spleen of the infected mice. We
195 observed a high copy of viral RNA both in liver (Fig. 4E) and spleen (Fig. 4F) tissues. We also
196 observed a decrease in the platelet count, as previously reported to occur during dengue
197 infection. As shown in Fig (S9A), a decrease in the platelet count was seen in G1 vs G2 and G3
198 however, we did not observe any significant difference in G2 vs G3. WBC and Hematocrit
199 measurement was also carried out but no significant differences in G2 vs G3 groups (Fig. S9A
200 and S9B) were observed.
201
202 **SARS-CoV-2 spike antibodies cross-react with DENV-2**
203 We wanted to check if the available sera/ antibodies cross react with DENV-2. To do that,
204 SARS-CoV-2 anti-spike polyclonal antibody raised in rabbit (P1R) and mice (MSer) (obtained
205 from BEI resources USA) were analyzed for cross-reactivity with DENV-2. Using confocal
206 microscopy, we observed that both showed a significant cross-reactivity with an average (MFI)
207 of 13·2 for P1R and 13·4 for MSer (Fig. 5A-B). Mouse Monoclonal antibodies against SARS-
208 CoV-2, 1A9 (MFI of 7.4) and MM41 (MFI of 1.57), also showed cross-reactivity with DENV-
209 2. The positive-control, 4G2 (pan-flavivirus-anti-envelope antibody), showed MFI of 18·28
210 whereas the Negative-control, anti-Rabies monoclonal (Rabishield®), showed no reactivity
211 with DENV-2. The binding kinetics of 1A9 (SARS-CoV-2 spike antibody) showed a high
212 affinity to DENV-2 Envelope with a dissociation constant (KD) of 4·84 μM (Fig. 5C ii-iii)
213 using Bio-Layer Interferometry (BLI).
214
215 **SARS-CoV-2 spike antibodies enhance DENV-2 infection**
216 Since DENV is endemic to India pre-existing anti-DENV antibodies may be responsible for the
217 observed ADE. To rule out this possibility, we further tested commercially available
218 monoclonal and polyclonal antibodies and sera raised in-house against the SARS-CoV-2 spike

219 and RBD for their potential to enhance the DENV-2 infection (Table-S6). All of the tested
220 antibodies (M1B, 1A9, MM41, P1R, M4B, M5B, Hser) enhanced DENV-2 infection (Fig. 6).
221 The RBD specific antibody (M5B) showed stronger enhancement compared to the antibody
222 against spike (MM41) with a dose-dependent increase in DENV-2 infection (Fig. 6A-B).
223 Similarly, hamster serum against purified SARS-CoV-2 spike protein also showed ADE of
224 DENV-2 infection in K562 cells (Fig. 6C). Monoclonal antibody against Rabies virus
225 (Negative-control), did not show any ADE of dengue infection in K562 cells (Fig. 6C). A
226 similar ADE of DENV infection was observed in U937 cells too (Fig. S10). Three monoclonal
227 antibodies – 4G2, 1A9, and M4B, showed significant ADE, as determined by the infectious
228 titer of the virus released in the culture supernatant from K562 cells (p-value<0·0001; Fig. S10).
229 Having established that there is an enhancement of DENV-2 infection due to anti-SARS-CoV-
230 2 antibodies, we next investigated whether it is time-dependent. We assessed ADE at 6 h, 18 h
231 and 36 h post-infection (Fig.S11). Mice (Mser) and hamster (Hser) sera, showed significant
232 ADE with respect to virus control (adjusted p-values Mser=0·0071 and Hser=0·0001), even at
233 6 hpi (Fig. S10). Although, we didn't observe a significant enhancement due to 4G2 and anti-
234 Spike monoclonals M3S and M2G at 6 hpi. At 18 hpi, a significant increase in the DENV-2
235 positive cells with respect to virus control was observed in 4G2 as well as M2G (Adjusted p-
236 value=0·0101), which further enhanced significantly at 36 hpi (Adjusted p-values 4G2=0·0001
237 and M2G=0·0035). The ADE in Hser reached saturation as early as 6 h (Adjusted p-
238 value<0·0001).
239
240 **Discussion:**
241 In this study, we demonstrate that SARS-CoV-2 antibodies cross-react with DENV-2 and
242 enhance DENV infection. A thorough *in silico* study indicated the high likeliness of cross-
243 reactivity of SARS-CoV-2 spike antibodies with DENV-2 E protein. SARS-CoV-2 spike

244 protein is critical for viral entry into cells and is the major target not only for neutralizing
245 antibodies but also for infection-enhancing antibodies (20). The *in silico* results indicated that
246 there is a significant interaction of SARS-CoV-2 antibodies with DENV-2 dimeric E protein.
247 The binding free energy of SARS-CoV-2 antibodies for example, CR3022 (6W7Y), S2E12 ab
248 (7K45) and DMAb2196 (8D8R), being comparable to the DENV-2 dimer specific antibody,
249 C8 (4UTA). These top three binders (SARS-CoV-2 specific antibodies) shared their interacting
250 interface with C8 antibody. The residues involved in the interaction of C8 antibody with
251 DENV-2 E, were also involved in the interaction of at-least one of the top three binders with
252 E-protein. The contributing residues which were found to be majorly stabilizing the interaction
253 of these top three SARS-CoV-2 antibodies with E-protein. We also observed that convalescent
254 plasma samples of SARS-CoV-2 recovered individuals, collected at three different time
255 intervals during COVID 19 pandemic, significantly enhanced the DENV-2 infection in cultured
256 Fc-receptor positive K562 and U937 cells. We observed an increased viral load as indicated by
257 FFU and also increased viral RNA levels in spleen and liver in AG129 mice group which had
258 SARS-CoV-2 antibodies. The finding in animals model strongly supported our *in silico* and *in*
259 *vitro* data which clearly showed that SARS-CoV-2 spike antibodies mediated enhancement of
260 dengue virus infection.
261 Our work supports the work published by others highlighting SARS-CoV-2 cross-reactivity
262 with dengue virus and false positivity with dengue serology (21) (22). We used the DENV-2
263 envelope protein for BLI and computational studies since it has been reported to have maximum
264 cross-reactivity with SARS-CoV-2 S1 specific antibodies (11). The dimeric DENV-2 E-protein
265 was used for docking studies as we intended to study the interaction of DENV-2 with SARS-
266 CoV-2 spike antibodies, which would happen before the viral entry, extracellularly and it's
267 known that the E-protein exists as a head-to-tail oriented homodimer on the surface of mature-
268 virions (23). All the residues involved in the interaction of the top three binders of SARS-CoV-

269 2 antibodies with E-protein when mapped, were majorly found to lie in the Domain-II and
270 fusion-loop of E-protein. It is well known that the antibodies against two epitopes of DENV are
271 strong mediators of ADE: prM epitopes (24) and fusion loop epitopes (25). The fusion loop
272 epitopes could be the ones, potentially involved in ADE. Multiple residues have been identified
273 from *in silico* interaction mining, among them few residues such as R73 (common among all),
274 T70, S72 (Domain-II), R99 and N103 (Fusion loop) and E311 (Domain-III) seem critical. These
275 residues put forth the possible avenue to explore further for epitope-based therapeutic
276 interventions. The BLI findings between dengue envelope protein and antibodies against
277 SARS-CoV-2 spike protein indicate a strong interaction with KD values in μM range.
278 The DENV-2 used for the *in vitro* assay was prepared in C6/36 cells and wasn't characterized
279 for the proportions of immature and mature-virions. It is well known that the virus prepared *in*
280 *vitro* in mosquito cells has a considerably greater number of immature virions as compared to
281 mammalian cells, probably due to differential furin-expression (26) (27). Also, it is recognized
282 that laboratory adapted DENV strains are more dynamic than clinical strains and expose cryptic
283 epitopes more easily (28). Thus our virus preparation might have major proportion of immature
284 virions but this probably won't change the fact that the ADE of DENV-infection would happen
285 since the viral heterogeneity in response to the natural DENV-infections is also well known
286 The antibody repertoire in the natural infections is known to have an abundance of poorly
287 neutralizing antibodies which are majorly generated in response to the immature conformations
288 (29), which is a result of incomplete furin processing, resulting in egress of immature-forms
289 along with and mature-forms of virions post-assembly (30) (31). Also, the fully mature-virions
290 have been reported to be less susceptible to neutralization by cross-reactive and heterotypic
291 immune sera than partially mature variants (29). Thus, the heterogeneity in the DENV-2
292 preparation used for the *in vitro* assays can be probably closely related to the natural infection
293 scenario. Although we did not have the history of patient's (SARS-CoV-2 Convalescent

294 samples) earlier infection from other dengue serotype which could have resulted in ADE in our
295 finding, we tested the commercially available SARS-CoV-2 antibodies and Spike-immunized
296 mice and hamster sera. Monoclonal and polyclonal antibodies raised against SARS-CoV-2
297 showed an increased DENV-2 infection in both cell-based models which re-confirms our
298 observations. Due to limitation on dengue virus serotypes, we only tested ADE against Dengue
299 serotype 2 (NGC strain and Clinical isolate (Indi-60) strain) but we believe that we will have
300 similar ADE effect as all the dengue serotypes are very closely antigenically related. However,
301 in the animal experiment, the platelet, WBC counts and hematocrit levels were not significantly
302 affected between mice given dengue (G2) and SARS CoV-2 + DENV (G3). As these
303 parameters are associated with disease severity which could explain why we did not observe
304 dengue severity during the SARS-CoV-2 pandemic which are promoting us to dig more deeper
305 and further studies to find the missing links. We also observed an increase in dengue viral load
306 in G3 (SARS CoV-2 + DENV infected) group mice as compared to G2 (dengue infected) group
307 mice, that might be indicating an increase in the number of the symptomatic cases in endemic
308 population rather asymptomatic cases. It is still not clear if there was underreporting or reduced
309 testing for dengue during the peak SARS-CoV-2 pandemic as the clinical symptoms of both
310 viruses are very similar. Our understanding is still limited and future studies might shed some
311 light on the this.
312 The limitation of the study is the availability of the pre-pandemic clinical samples like
313 plasma/Serum or PBMCs, which could have provided a better insight and might have shed
314 some light on why these all are not leading to dengue severity in the real-world scenario. We
315 tried to overcome this using the animal model but a clinical sample would have been better
316 comparator.
317 Based on the current finding from *in silico, in vitro and in vivo* experiments, the study suggest
318 that SARS-CoV-2 spike directed antibodies cross reacts with dengue envelope protein and

319 enhance dengue viral load in AG129 experimental mice. Our findings signify the importance
320 of the cross reactivity and viral interactions in endemic regions where more than one virus is
321 circulating at the same time. Understanding the viral interactions during the co-circulation/Co-
322 infections needed more research in future to understand how they pose vaccine development
323 challenges and will impact on public health. These things will also pose significant challenges
324 on surveillance and/or vaccine running programs which might provide a false positivity due to
325 viral cross reactivity. So having an assay which can clearly differentiate the viral infection will
326 be more beneficial approach in future.
327

328 **Materials and Methods:**

329 **Molecular docking of DENV-2 Envelope glycoprotein and SARS- CoV-2 antibodies:**

330 **Curation of data:**

331 X-ray crystal structures of DENV-2 envelope glycoprotein (PDB ID:4UT6) (32) and SARS-
332 CoV-2 antibodies were curated from RCSB in PDB format (http://www.rcsb.org/pdb). These
333 crystal structures along with their corresponding resolution values, and are summarized in –
334 Table-S1. Crystal structure of antibodies were curated by removal of spike protein, water
335 molecules and metal ions using UCSF Chimera 1·15 (33). All structures were prepared using
336 Maestro's Protein Preparation Wizard module (Schrödinger Release 2020-1) (34). The
337 hydrogens and bond orders were added, missing side-chains and loops were filled by Prime
338 (34). The hydrogen bond (HB) optimization and restrained minimizations were also done for
339 the systems using force field OPLS4 (35).

340 **Protein-Antibody docking and choosing the best pose:**

341 Protein-protein interactions govern various aspects of structural and functional cellular
342 mechanisms, and their elucidation is crucial for a better understanding of biological processes.
343 All the prepared SARS-CoV-2 antibodies, along with controls i.e positive (pdb-id:4UTA) and
344 negative control (pdb-id:7U9G) were docked on prepared DENV2 E protein structure by
345 masking non-CDR regions of antibodies. The Chothia definition is used for the CDR region.
346 Multiple docking methods were used to minimize the biases by including HDOCK (36),
347 pyDock (37) and Piper program (38). The rationale for implementing multiple docking
348 programs was to obtain the consensus results from all three tools and to remove any false-
349 positive outcomes. Best poses were chosen from docked models on the basis of their docking
350 score, cluster size (39) and reported paratope residues (40) (41) (42).

351 **Thermodynamic quantification using Molecular Mechanics-Generalized Born Surface**
352 **Area (MM-GBSA):**

353 The binding free energy of protein and antibody complexes was carried out in Prime MM-
354 GBSA (Molecular Mechanics Generalized Born Surface Area) by Prime (43) module of
355 Schrodinger suite. We used the VSGB solvation model and OPLS4 force field. The binding
356 free energy is calculated by: MMGBSA dG Bind (NS) = Complex – Receptor (from optimized
357 complex) – Ligand (from optimized complex) = MMGBSA dG Bind–Rec Strain–Lig Strain,
358 Where, Rec Strain = Receptor (from optimized complex) – Receptor, Lig Strain = Ligand (from
359 optimized complex) – Ligand, MMGBSA dG Bind = Complex – Receptor – Ligand, NS = no
360 strain.

361 **Figures:**

362 All figures were generated using VMD (V.1·9·1) (44) and graphs were generated using the
363 XMGRACE (Version 5·1·19) (42).

364 **Cells:**

365 Human myeloid cell lines K562 (ATCC CCL-243) and U937 (ATCC CRL-1593.2) were
366 cultured in Iscove's Modified Dulbecco's media (IMDM, HIMEDIA) and Roswell Park
367 Memorial Institute (RPMI, Gibco) 1640 respectively. African Green Monkey cell line Vero E6
368 (NCCS, India) was maintained in Dulbecco's Modified Eagle Medium (DMEM, HIMEDIA)
369 while A. albopictus cell line C6/36 (NCCS, India) was cultivated in Leibovitz's L-15 Medium
370 (HIMEDIA). All the cells were maintained in respective media supplemented with 100 U/ml
371 of penicillin, 100 µg/ml of streptomycin (HIMEDIA), and 10% Fetal Bovine Serum
372 (HIMEDIA). C6/36 cells were maintained at 28°C (ESCO incubator) without CO_2 while the
373 other cells were grown in a humidified 37°C incubator (Thermo Fisher Scientific) with 5%
374 CO_2.

375 **Virus stocks:**

376 Dengue virus serotype 2 (NGC strain) and (P8-P23085 INDI-60) were propagated in C6/36
377 cells and it was used for all the assays. The cells at a confluency of 60-70% were infected with
378 Dengue virus at a multiplicity of infection (MOI) of 0·1 using inoculum prepared in L-15
379 medium supplemented with 2% FBS. It was incubated with cells for 2 h at 28°C with
380 intermittent rocking. Subsequently, the cells were washed and incubated with L-15 medium
381 with 10% FBS. Culture supernatant was harvested at 5 dpi, clarified by centrifugation at 129
382 ×*g* at room temperature and concentrated using centrifugal ultrafiltration (Amicon® Ultra
383 centrifugal filter (100 kDa), ACS510024 from Millipore, Darmstadt, Germany) at 3220 ×*g* for
384 10 min for every 15 ml of supernatant. The infectious titer of the virus was determined by a
385 focus-forming unit (FFU) assay performed in Vero E6 cells.

386 The three variants of SARS-CoV-2, original Wuhan (USA-WA1/2020, Genbank: MN985325),
387 B·1·617·2 (δ-variant) known as THSTI_287 (GenBank: MZ356566·1), and Omicron

388 BA·1(GISAID accession no.: EPI_ISL_8764350) were propagated in Vero E6 cells. Cells were
389 infected with 0·1 MOI of virus inoculum and incubated for 1 h with shaking at 37°C. Virus
390 supernatant was harvested at 48 hpi, filtered, and stored at -80°C. The infective titer was
391 determined by titration on Vero E6 cells using the $TCID_{50}$ method (45). These virus stocks were
392 used for neutralization assays.

393 **Serum samples and Antibodies:**

394 We selected a group of convalescent plasma samples (n=48) collected at three different time
395 intervals during COVID-19 pandemic in India. They are defined as follows: the first interval
396 was from May 2020 to January 2021, second interval from May 2021 to June 2021, third
397 interval from February 2022 to April 2022. The clinical details of the samples are given in the
398 Table S1. The pan flavivirus, anti-envelope mAb, 4G2 was purified inhouse from HB112
399 hybridoma cells. SARS-CoV-2 spike (S2 specific) antibody 1A9 was purchased from Gentex
400 while Anti- Recombinant SARS-CoV-2 Spike Protein (whole spike) Sino 4059-MM41 was
401 purchased from Sino Biologicals. Other SARS CoV2-related antibodies M1B, M4B, M5B, P1R
402 were obtained from BEI resources, USA. SARS CoV2 infected mice and hamster serum were
403 generated inhouse. Rabies Human monoclonal antibody, Rabishield®-100 (Serum Institute of
404 India), was purchased from the pharmacy. All the details regarding commercial antibodies/
405 serum are mentioned in - Table S2.

406 **Confocal microscopy:**

407 0.5 x 10^6 C6/36 cells from an exponentially growing culture were seeded on grass cover slips
408 followed by DENV-2 at 1.0 MOI. At 48 h post-infection the cells were fixed with 3.7%
409 paraformaldehyde (PFA) and permeabilized using 0.1% Triton-X-100. The cells were immune-
410 stained with primary antibody and fluor-conjugated secondary antibodies. Subsequently,

411 coverslips were mounted onto glass slides using ProLong Gold Antifade Mountant
412 supplemented with DAPI. Fluorescence was observed under 60X magnification using a
413 FLUOVIEW FV3000 confocal microscope (Olympus). The mean fluorescence intensity (MFI)
414 was calculated using images from 10 fields per slide with 7 cells per field (at least 70 data
415 points). Statistical analysis employed One-way ANOVA followed by Dunnett's test, comparing
416 to the negative control (Rabishield).

417 **Binding kinetics using Biolayer Interferometry (BLI):**

418 BLI studies were performed on an Octet RED 96 instrument at 24°C with shaking at 1000 rpm
419 (ForteBIO). For DENV-2 Envelope protein, the buffer composition was 50mM Tris, 150mM
420 NaCl, 0.5% glycerol, pH 8.0. Whereas, for SARS-CoV-2 Spike protein, phosphate buffered
421 saline, pH 7.4 was used. Sensors were in the respective kinetic buffer (46). For studying binding
422 kinetics with protein E, antibodies at a concentration of 5 µg/ml were loaded onto the sensors
423 (AHC (Anti-hIgG Fc Capture) for CR3022 and C8, protein G (for 1A9 antibody)) DENV E
424 dimeric protein was diluted serially three-fold (starting with 6000nM) and Spike trimeric
425 protein was diluted 2-fold (starting with 600nM) in their respective kinetic buffers. The
426 designed experiment started with a baseline (100Sec), followed by 3 cycles of neutralization
427 and regeneration and again a baseline (100Sec). After this step, antibody loading was performed
428 (700sec) onto all the 5 sensors. After the loading step, another baseline (baseline2, 60sec),
429 Association was performed after the 2nd baseline step for 300sec, followed by 300sec
430 dissociation.

431 Here the 5th sensor was used as reference where no analyte was used, where the analyte
432 concentration was kept 0nM. The same sensor during the data processing was assigned as
433 reference well (change well type-reference well) and same wells; reference well, were
434 subtracted from the raw data. Here the ligand and analyte dilution as well as the whole

435 experiment was performed in the respective kinetic buffers. The binding responses were
436 calculated and fitting globally with a 1:1 binding model using ForteBio's Data Analysis
437 software 10·1. The data was considered validated if $X^2 < 0·5$.

438 **Antibody-dependent Enhancement (ADE) Assay:**

439 Convalescent Serum samples (15 µl), Purified IgG antibodies (10 µg) and commercial
440 antibodies (at various concentrations) were diluted in plain Iscove's Modified Dulbecco's
441 Medium (IMDM) to a total volume of 100 µl. Subsequently, 100 µl of virus dilution was added,
442 and the mixture was incubated at 37°C for 1 h. The virus-antibody complexes were then allowed
443 to infect 1 x 10^6 cells K562/U937 cells for 2 h at an MOI 1. After infection the cells were
444 washed and incubated in IMDM-2% FBS at 37°C, 5% CO_2 for 36 h. Subsequently, cells were
445 fixed using 4% PFA, permeabilized with 0.1% Triton X-100, immune-stained with purified
446 4G2 (dilution 1:200), and Alexa-Fluor 488 conjugated anti-mouse (dilution 1:500). The number
447 of cells positive for DENV antigen was quantified by flow cytometry.

448 **Isolation and Purification of IgG from Serum samples**

449 Serum sample was centrifuged at 10,000 x g at 4 °C for 10 min followed by adding 1 part of 1
450 M Tris-HCl, pH 8.0 to 10 parts of serum sample, to adjust the pH. Drop by drop, saturated
451 ammonium sulphate solution up to 45% saturation was added to it and it was stirred for 1 h.
452 Serum sample was again centrifuged at 10,000 x g at 4 °C for 10 min and supernatant was
453 discarded. Pellet was dissolved in minimum volume of the desalting column buffer. Sephadex
454 G-25 column was once cleaned with distilled water and then equilibrated with 10-15 ml of
455 binding buffer. The sample was loaded onto the column and flowthrough was collected in a
456 fresh 15ml falcon. Binding buffer (5-10 ml) was again passed through the column and about
457 1-2 ml of flowthrough was collected in the same falcon tube. To separate the IgG, protein G

458 column was rinsed with ethanol and then distilled water. Collection tubes with 50 µl of 1.0 M
459 dibasic sodium phosphate was prepared to ensure that the final pH of the collected samples is
460 close to neutral. The packed column was washed with five column volumes (~25 ml) distilled
461 water to remove the slurry storage medium. Column was equilibrated with five to ten column
462 volumes of 50mM sodium phosphate, pH 7.0 and 500 mM NaCl (binding buffer). Pre-treated
463 sample was loaded on the equilibrated column. Column was washed with~ 25 ml binding buffer
464 followed by elution with 5 column volumes of elution buffer. Fractions of 500 µl were collected
465 into the collection tubes containing the neutralizing buffer. The fractions were analysed by
466 absorbance at 280 nm in a spectrophotometer to measure protein concentration and SDS-PAGE
467 to confirm purity of IgG.

468 **Flow Cytometry Analysis:**

469 Flow cytometry was conducted using a BD FACS Canto II flow cytometer (BD Biosciences)
470 with 20,000 cells acquired per sample through FACS Diva software. FlowJo v10.8.1 was used
471 for analysis. Live cells were gated based on FSC and SSC, followed by singlet determination
472 using FSC-A vs FSC-H gate. Dengue virus-positive cells were gated on the FITC channel using
473 singlet population. FITC voltage was set using isotype control. Fcγ receptor expression was
474 assessed with anti-CD64 (Alexa Fluor 700), anti-CD32 (PE), and anti-CD16 (APC) antibodies
475 in K562 and U937 cells. Statistical analysis was conducted in GraphPad Prism 8.

476 **Live Virus Neutralization Assay:**

477 Two-fold serial dilutions of heat-inactivated plasma samples were mixed with 100 $TCID_{50}$ of
478 SARS-CoV-2 virus and subsequently allowed to infect Vero E6 monolayers. After incubation
479 for 72 h at 37°C with 5% CO_2, the degree of CPE was qualitatively determined under a
480 microscope. Absence of CPE indicated virus neutralization, and the highest dilution that

481 completely prevented emergence of CPE was considered as the neutralization titer. For plasma
482 samples collected during-the third interval, cells were fixed 24 h post-infection and immune-
483 stained using antibody against the SARS-CoV-2 Nucleocapsid protein (1:2000, 4H2,
484 Genscript), followed by Alexa 488 conjugated anti-mouse antibody (1:500, Invitrogen).
485 Fluorescent foci were quantified by AID iSpot Reader with AID EliSpot 8.0 iSpot software.

486 **Detection of DENV RNA using Quantitative RT-PCR:**

487 Total RNA from 1 x 10^6 K562 cells was extracted using the standard TRIzol method. RNA was
488 quantitated using Nanodrop (Thermofisher Scientific) and 300 ng RNA was used for qPCR
489 using a one-step RT-PCR kit (SOLIScript® 1-step Probe kit, Solis Biodyne) following the
490 manufacturer's protocol for detection of DENV2 RNA. GAPDH was used as an internal
491 control. Fold change in DENV2 RNA copies was calculated with respect to GAPDH. The
492 details regarding primer and probe sequences are given in Table S7.

493 **Focus forming unit (FFU) assay**

494 FFU assay was carried out to determine the virus titer in the serum of DENV2 infected AG129
495 mice with slight modifications. Vero E6 cells were seeded at a density of 0.01x10^6 cells/well in
496 a 96-well black/clear bottom plate and cells were allowed to reach 80% confluency. At 80%
497 confluency 100 µl of 10-fold serially diluted serum in media with 2% FBS was added to the
498 wells and incubated. After 2 hr, serum was removed, fresh media with 2% FBS was added and
499 incubated for 24 hr at 37° C in 5% CO_2. Following that cells were fixed with 2% PFA and the
500 immunostaining for virus detection was performed using mAb 4G2 (pan-DENV anti-envelope
501 antibody), followed by secondary antibody, goat anti-mouse IgG, AF488 conjugated
502 (Invitrogen) prepared in permeabilization buffer (0.1% triton x100 with 2%BSA in PBS). The
503 foci were visualized and counted using fluorescence microscope.

504 **Mouse Infection**

505 The AG129 (IFNα/β/γR -/- 129/Sv) mice were obtained from the Jackson laboratory, USA
506 and maintained in small animal facility (SAF), RCB, Faridabad, India. All experiments with
507 AG129 mice were performed in 6-8 weeks old mice of either sex. One group of mice were
508 treated (one-time through intranasal route) with human ACE2 adenovirus using $2.5x10^8$ PFU
509 for transient expression of hACE2 in lungs and respiratory track. After five days mice were
510 infected with SARS-CoV-2 via nasal route inoculation using $1x10^5$ PFU virus. Mice were
511 bled at day7, 14 and 21 post SARS-CoV-2 infection to measure the antibodies against SARS-
512 CoV-2. At day 21 both the groups were challenged with $1x10^4$ FFU mouse-adapted DENV2
513 (P8-P23085 INDI-60) and were euthanized on the moribund state.

514 **Quantitative real time PCR**

515 Total RNA from the mice tissues was extracted using RNAiso (Takara Bio, Japan) followed by
516 phenol-chloroform treatment. The first strand cDNA was synthesized from 1µg RNA using
517 cDNA synthesis kit (BioRad, USA) as per manufacturer's protocol. The cDNA was used for
518 real-time PCR using SYBR green supermix (BioRad) in an Applied Biosystems Quant
519 Studio™ 6 Flex Real-Time PCR System. The primers set used for detection of the respective
520 genes are given in Table S8.

521 **Statistical analysis:**

522 Experimental values were represented as mean ± standard deviation (SD). Statistical analysis
523 was done using the ordinary one-way ANOVA followed by Dunnett's multiple comparison
524 test, using GraphPad Prism version 8·4·2. Differences were considered significant at p-value <
525 0·05.

526

527 **Acknowledgements:**

528 The following reagent was obtained through BEI Resources, NIAID, NIH: SARS-Related
529 Coronavirus 2, Isolate USA-WA1/2020, NR-52281, Monoclonal Anti-SARS-Related
530 Coronavirus 2 Spike Glycoprotein, Clone 1-3D7 (produced *in vitro*), NR-56488, Monoclonal
531 Anti-SARS-Related Coronavirus 2 Spike Glycoprotein Receptor Binding Domain-(RBD),
532 Clone 2TP1C3 (produced *in vitro*), NR-55296, Polyclonal Anti-SARS-Related Coronavirus 2
533 Spike Glycoprotein (IgG, Rabbit), NR-52947." The RBD is proprietary reagents with IP No.
534 202011018845, we thank Dr. Barney Graham (VRC/NIAID/NIH) for providing us with spike
535 construct (SARS-2-CoV S 2P). We would like to thank Prof. Shinjini Bhatnagar, Prof. Pramod
536 Garg and Prof. Jayanta Bhattacharya from THSTI for critically reviewing the manuscript,
537 ABSL3 facility committee and staff for their help and support. This research has been
538 conducted with the significant contribution and expertise of THSTI, NCR Biotech Science
539 Cluster BIOREPOSITORY and DBT India Consortium".

540 DBT India Consortium**, ** Name of all the collaborating Institutes/ Hospitals: Translational
541 Health Science Technology Institute, Clinical partners: Maulana Azad Medical College, Lok
542 Nayak Jai Prakash Hospital, and Lady Hardinge Medical College in Delhi, ESI Medical College
543 Hospital, Faridabad, Civil Hospital, Gurugram, Haryana; Civil Hospital, Palwal, Haryana; Al-
544 Falah School of Medical Science & Research Centre and Hospital, Dhauj, Haryana; Medanta
545 Hospital, Gurugram; Shaheed Hasan Khan Mewati Government Medical College, Nalhar,
546 Haryana.

547

548 **Data availability:**

549 All the data are presented in this manuscript. The virus strains used in this study have the
550 following accession numbers: original Wuhan (USA-WA1/2020, Genbank: MN985325),

551 B·1·617·2 (δ-variant) known as THSTI_287 (GenBank: MZ356566·1), and Omicron BA·1
552 (GISAID accession no.: EPI_ISL_8764350) Source data are provided with this paper.

553 **Author Contributions:**

554 SM conceptualized the idea. SM, SB, SA, TrS and PG coordinated the research activity. KJ
555 and SS contributed to designing and execution of viral assays. KJ, SS, GS, NB, TS, MT, JK,
556 DKR, BL, SK, PS, SK, VP, S, LK and VG contributed to data curation, investigation and
557 methodology. KJ, SS, TRA, GJ, GS, SB, SA, TrS, PG and SM contributed to formal analysis.
558 SS, SR, MG, PK, NW, RT, SB, TrS, SA and SM provided resources. KJ, SS, TRA, GJ, TrS,
559 PK, NW, RT, SB, SA, PG and SM contributed to writing, review & editing the draft. All authors
560 had full access to all the data in the study and had final responsibility for the decision to submit
561 for publication.

562

563 **Ethics statement**

564 We obtained the approval from the Institutional Bio-Safety Committee and Review
565 Committee on Genetic Manipulation (RCGM), for *in vitro* and *in vivo* work, prior to
566 conducting the studies: (IBSC#495/2023), RCGM (No.-BT/IBKP/137/2020), RCGM
567 (No.BT/IBKP/053/ 2020).

568

569 **Disclosure statement**

570 The Author declares no conflict of interest.

571

572 **Funding:**

573 The current research is funded by the Translational Research Program Grant,
574 BT/PR30159/MED/15/188/2018, THSTI Core (Intramural P417) and the Bill and Melinda
575 Gates Foundation GIISER-South Asia (INV-030592). The computational work was supported

576 by the national network project (NNP-BT/PR40189/BTIS/137/50/2022), DBT. The work on
577 dengue envelope proteins was done with support of funding received from NBM (National
578 Biopharma Mission) scheme of BIRAC (Biotechnology Industry Research Assistance
579 Council), India (BT/NBM099/02/18) (2019-2023). SK acknowledge NBM BIRAC for his
580 fellowship support.
581
582

583 **Reference:**

584

585 1. WHO. WHO, Fact sheets / Detail / Dengue and severe dengue 2023 [cited 2023 11th
586 December]. Available from: https://www.who.int/news-room/fact-sheets/detail/dengue-
587 and-severe-dengue.
588 2. Lee MF, Voon GZ, Lim HX, Chua ML, Poh CL. Innate and adaptive immune evasion by
589 dengue virus. Front Cell Infect Microbiol. 2022;12:1004608. Epub 2022/10/04. doi:
590 10.3389/fcimb.2022.1004608. PubMed PMID: 36189361; PubMed Central PMCID:
591 PMC9523788.
592 3. Pierson TC, Diamond MS. A game of numbers: the stoichiometry of antibody-
593 mediated neutralization of flavivirus infection. Prog Mol Biol Transl Sci. 2015;129:141–66.
594 Epub 2015/01/18. doi: 10.1016/bs.pmbts.2014.10.005. PubMed PMID: 25595803; PubMed
595 Central PMCID: PMC4910618.
596 4. Khan S, Akbar SMF, Yahiro T, Mahtab MA, Kimitsuki K, Hashimoto T, et al. Dengue
597 Infections during COVID-19 Period: Reflection of Reality or Elusive Data Due to Effect of
598 Pandemic. Int J Environ Res Public Health. 2022;19(17). Epub 2022/09/10. doi:
599 10.3390/ijerph191710768. PubMed PMID: 36078486; PubMed Central PMCID:
600 PMC9518125.
601 5. Khan S, Akbar SMF, Nishizono A. Co-existence of a pandemic (SARS-CoV-2) and an
602 epidemic (Dengue virus) at some focal points in Southeast Asia: Pathogenic importance,
603 preparedness, and strategy of tackling. Lancet Reg Health Southeast Asia. 2022;4:100046.
604 Epub 2022/07/26. doi: 10.1016/j.lansea.2022.100046. PubMed PMID: 35873345; PubMed
605 Central PMCID: PMC9296506 interest.
606 6. Lu X, Bambrick H, Pongsumpun P, Dhewantara PW, Toan DTT, Hu W. Dengue
607 outbreaks in the COVID-19 era: Alarm raised for Asia. PLoS Negl Trop Dis.
608 2021;15(10):e0009778. Epub 2021/10/09. doi: 10.1371/journal.pntd.0009778. PubMed
609 PMID: 34624031; PubMed Central PMCID: PMC8500420.
610 7. Manna S, Satapathy P, Bora I, Padhi BK. Dengue outbreaks in South Asia amid Covid-
611 19: Epidemiology, transmission, and mitigation strategies. Front Public Health.
612 2022;10:1060043. Epub 2023/01/03. doi: 10.3389/fpubh.2022.1060043. PubMed PMID:
613 36589966; PubMed Central PMCID: PMC9797821.
614 8. Oladipo HJ, Rabiu I, Tajudeen YA. Dengue virus and SARS-CoV-2 Co-infection
615 dynamics: An emerging threat among African countries. Ann Med Surg (Lond).
616 2022;82:104398. Epub 2022/08/30. doi: 10.1016/j.amsu.2022.104398. PubMed PMID:
617 36035770; PubMed Central PMCID: PMC9394095.
618 9. Prapty C, Rahmat R, Araf Y, Shounak SK, Noor AA, Rahaman TI, et al. SARS-CoV-2 and
619 dengue virus co-infection: Epidemiology, pathogenesis, diagnosis, treatment, and
620 management. Rev Med Virol. 2023;33(1):e2340. Epub 2022/03/04. doi: 10.1002/rmv.2340.
621 PubMed PMID: 35238422; PubMed Central PMCID: PMC9111128.
622 10. Rana MS, Usman M, Alam MM, Ikram A, Salman M, Umair M. Impact of previous
623 SARS-CoV-2 infection on the rate of mortality in dengue. A preliminary report from Pakistan.
624 J Infect. 2022;84(5):722–46. Epub 2022/01/27. doi: 10.1016/j.jinf.2022.01.027. PubMed
625 PMID: 35081438; PubMed Central PMCID: PMC8783977 of interest.
626 11. Masyeni S, Santoso MS, Widyaningsih PD, Asmara DW, Nainu F, Harapan H, et al.
627 Serological cross-reaction and coinfection of dengue and COVID-19 in Asia: Experience from
628 Indonesia. Int J Infect Dis. 2021;102:152–4. Epub 2020/10/30. doi:

629 10.1016/j.ijid.2020.10.043. PubMed PMID: 33115680; PubMed Central PMCID:
630 PMC7585717.
631 12. Alla D, Alla SSM, Vempati R, Bhatt H, Sultana Q, Bhatt S, et al. Dengue & COVID-19: A
632 Comparison and the Challenges at Hand. Cureus. 2022;14(11):e31877. Epub 2022/12/30.
633 doi: 10.7759/cureus.31877. PubMed PMID: 36579259; PubMed Central PMCID:
634 PMC9792364.
635 13. Digwo DC, Elebe CP, Chigor VN, Madueke SN, Ezeh CK, Ike AC. Occurrence of False-
636 Positive Tests and Cross-reactions Between COVID-19 and Dengue With Implications During
637 Diagnosis: A Mixed Evidence Synthesis. Infectious Microbes & Diseases. 2023;5(2):64–75.
638 doi: 10.1097/im9.0000000000000116. PubMed PMID: 02123149-202306000-00004.
639 14. Ulrich H, Pillat MM, Tarnok A. Dengue Fever, COVID-19 (SARS-CoV-2), and Antibody-
640 Dependent Enhancement (ADE): A Perspective. Cytometry A. 2020;97(7):662–7. Epub
641 2020/06/09. doi: 10.1002/cyto.a.24047. PubMed PMID: 32506725; PubMed Central PMCID:
642 PMC7300451.
643 15. Cheng YL, Chao CH, Lai YC, Hsieh KH, Wang JR, Wan SW, et al. Antibodies against the
644 SARS-CoV-2 S1-RBD cross-react with dengue virus and hinder dengue pathogenesis. Front
645 Immunol. 2022;13:941923. Epub 2022/09/02. doi: 10.3389/fimmu.2022.941923. PubMed
646 PMID: 36045680; PubMed Central PMCID: PMC9420930.
647 16. Nath H, Mallick A, Roy S, Kayal T, Ranjan S, Sengupta S, et al. COVID-19 serum can be
648 cross-reactive and neutralizing against the dengue virus, as observed by the dengue virus
649 neutralization test. Int J Infect Dis. 2022;122:576–84. Epub 2022/07/11. doi:
650 10.1016/j.ijid.2022.07.013. PubMed PMID: 35811081; PubMed Central PMCID:
651 PMC9262656.
652 17. El-Qushayri AE, Kamel AMA, Reda A, Ghozy S. Does dengue and COVID-19 co-
653 infection have worse outcomes? A systematic review of current evidence. Rev Med Virol.
654 2022;32(5):e2339. Epub 2022/02/26. doi: 10.1002/rmv.2339. PubMed PMID: 35213764;
655 PubMed Central PMCID: PMC9111070.
656 18. Srivastava M, Suri C, Singh M, Mathur R, Asthana S. Molecular dynamics simulation
657 reveals the possible druggable hot-spots of USP7. Oncotarget. 2018;9(76):34289–305. Epub
658 2018/10/23. doi: 10.18632/oncotarget.26136. PubMed PMID: 30344943; PubMed Central
659 PMCID: PMC6188144.
660 19. Littaua R, Kurane I, Ennis FA. Human IgG Fc receptor II mediates antibody-dependent
661 enhancement of dengue virus infection. J Immunol. 1990;144(8):3183–6. Epub 1990/04/15.
662 PubMed PMID: 2139079.
663 20. Wahala WM, Silva AM. The human antibody response to dengue virus infection.
664 Viruses. 2011;3(12):2374–95. Epub 2012/02/23. doi: 10.3390/v3122374. PubMed PMID:
665 22355444; PubMed Central PMCID: PMC3280510.
666 21. Yan G, Lee CK, Lam LTM, Yan B, Chua YX, Lim AYN, et al. Covert COVID-19 and false-
667 positive dengue serology in Singapore. Lancet Infect Dis. 2020;20(5):536. Epub 2020/03/08.
668 doi: 10.1016/S1473-3099(20)30158-4. PubMed PMID: 32145189; PubMed Central PMCID:
669 PMC7128937.
670 22. Lustig Y, Keler S, Kolodny R, Ben-Tal N, Atias-Varon D, Shlush E, et al. Potential
671 Antigenic Cross-reactivity Between Severe Acute Respiratory Syndrome Coronavirus 2 (SARS-
672 CoV-2) and Dengue Viruses. Clin Infect Dis. 2021;73(7):e2444–e9. Epub 2020/08/17. doi:
673 10.1093/cid/ciaa1207. PubMed PMID: 32797228; PubMed Central PMCID: PMC7454334.
674 23. Modis Y, Ogata S, Clements D, Harrison SC. A ligand-binding pocket in the dengue
675 virus envelope glycoprotein. Proc Natl Acad Sci U S A. 2003;100(12):6986–91. Epub

676 2003/05/22. doi: 10.1073/pnas.0832193100. PubMed PMID: 12759475; PubMed Central
677 PMCID: PMC165817.
678 24. Rodenhuis-Zybert IA, van der Schaar HM, da Silva Voorham JM, van der Ende-
679 Metselaar H, Lei HY, Wilschut J, et al. Immature dengue virus: a veiled pathogen? PLoS
680 Pathog. 2010;6(1):e1000718. Epub 2010/01/12. doi: 10.1371/journal.ppat.1000718.
681 PubMed PMID: 20062797; PubMed Central PMCID: PMC2798752.
682 25. de Alwis R, Williams KL, Schmid MA, Lai CY, Patel B, Smith SA, et al. Dengue viruses
683 are enhanced by distinct populations of serotype cross-reactive antibodies in human
684 immune sera. PLoS Pathog. 2014;10(10):e1004386. Epub 2014/10/03. doi:
685 10.1371/journal.ppat.1004386. PubMed PMID: 25275316; PubMed Central PMCID:
686 PMC4183589.
687 26. Murray JM, Aaskov JG, Wright PJ. Processing of the dengue virus type 2 proteins prM
688 and C-prM. J Gen Virol. 1993;74 (Pt 2):175–82. Epub 1993/02/01. doi: 10.1099/0022-1317-
689 74-2-175. PubMed PMID: 8429301.
690 27. Davis CW, Nguyen HY, Hanna SL, Sanchez MD, Doms RW, Pierson TC. West Nile virus
691 discriminates between DC-SIGN and DC-SIGNR for cellular attachment and infection. J Virol.
692 2006;80(3):1290–301. Epub 2006/01/18. doi: 10.1128/JVI.80.3.1290-1301.2006. PubMed
693 PMID: 16415006; PubMed Central PMCID: PMC1346927.
694 28. Chaichana P, Okabayashi T, Puiprom O, Sasayama M, Sasaki T, Yamashita A, et al. Low
695 levels of antibody-dependent enhancement in vitro using viruses and plasma from dengue
696 patients. PLoS One. 2014;9(3):e92173. Epub 2014/03/20. doi:
697 10.1371/journal.pone.0092173. PubMed PMID: 24642752; PubMed Central PMCID:
698 PMC3958444.
699 29. Beltramello M, Williams KL, Simmons CP, Macagno A, Simonelli L, Quyen NT, et al.
700 The human immune response to Dengue virus is dominated by highly cross-reactive
701 antibodies endowed with neutralizing and enhancing activity. Cell Host Microbe.
702 2010;8(3):271–83. Epub 2010/09/14. doi: 10.1016/j.chom.2010.08.007. PubMed PMID:
703 20833378; PubMed Central PMCID: PMC3884547.
704 30. Pierson TC, Diamond MS. Degrees of maturity: the complex structure and biology of
705 flaviviruses. Curr Opin Virol. 2012;2(2):168–75. Epub 2012/03/27. doi:
706 10.1016/j.coviro.2012.02.011. PubMed PMID: 22445964; PubMed Central PMCID:
707 PMC3715965.
708 31. Cherrier MV, Kaufmann B, Nybakken GE, Lok SM, Warren JT, Chen BR, et al.
709 Structural basis for the preferential recognition of immature flaviviruses by a fusion-loop
710 antibody. EMBO J. 2009;28(20):3269–76. Epub 2009/08/29. doi: 10.1038/emboj.2009.245.
711 PubMed PMID: 19713934; PubMed Central PMCID: PMC2771083.
712 32. Rouvinski A, Guardado-Calvo P, Barba-Spaeth G, Duquerroy S, Vaney MC, Kikuti CM,
713 et al. Recognition determinants of broadly neutralizing human antibodies against dengue
714 viruses. Nature. 2015;520(7545):109–13. Epub 2015/01/13. doi: 10.1038/nature14130.
715 PubMed PMID: 25581790.
716 33. Pettersen EF, Goddard TD, Huang CC, Couch GS, Greenblatt DM, Meng EC, et al. UCSF
717 Chimera--a visualization system for exploratory research and analysis. J Comput Chem.
718 2004;25(13):1605–12. Epub 2004/07/21. doi: 10.1002/jcc.20084. PubMed PMID: 15264254.
719 34. Sastry GM, Adzhigirey M, Day T, Annabhimoju R, Sherman W. Protein and ligand
720 preparation: parameters, protocols, and influence on virtual screening enrichments. J
721 Comput Aided Mol Des. 2013;27(3):221–34. Epub 2013/04/13. doi: 10.1007/s10822-013-
722 9644-8. PubMed PMID: 23579614.

723 35. Lu C, Wu C, Ghoreishi D, Chen W, Wang L, Damm W, et al. OPLS4: Improving Force
724 Field Accuracy on Challenging Regimes of Chemical Space. J Chem Theory Comput.
725 2021;17(7):4291–300. Epub 2021/06/08. doi: 10.1021/acs.jctc.1c00302. PubMed PMID:
726 34096718.
727 36. Yan Y, Tao H, He J, Huang SY. The HDOCK server for integrated protein-protein
728 docking. Nat Protoc. 2020;15(5):1829–52. Epub 2020/04/10. doi: 10.1038/s41596-020-0312-
729 x. PubMed PMID: 32269383.
730 37. Pallara C, Jimenez-Garcia B, Romero M, Moal IH, Fernandez-Recio J. pyDock scoring
731 for the new modeling challenges in docking: Protein-peptide, homo-multimers, and domain-
732 domain interactions. Proteins. 2017;85(3):487–96. Epub 2016/10/26. doi:
733 10.1002/prot.25184. PubMed PMID: 27701776.
734 38. Kozakov D, Brenke R, Comeau SR, Vajda S. PIPER: an FFT-based protein docking
735 program with pairwise potentials. Proteins. 2006;65(2):392–406. Epub 2006/08/26. doi:
736 10.1002/prot.21117. PubMed PMID: 16933295.
737 39. Lorenzen S, Zhang Y. Identification of near-native structures by clustering protein
738 docking conformations. Proteins. 2007;68(1):187–94. Epub 2007/04/03. doi:
739 10.1002/prot.21442. PubMed PMID: 17397057.
740 40. Zhang L, Cao L, Gao XS, Zheng BY, Deng YQ, Li JX, et al. A proof of concept for
741 neutralizing antibody-guided vaccine design against SARS-CoV-2. Natl Sci Rev.
742 2021;8(8):nwab053. Epub 2021/10/23. doi: 10.1093/nsr/nwab053. PubMed PMID:
743 34676098; PubMed Central PMCID: PMC8083607.
744 41. Shan S, Mok CK, Zhang S, Lan J, Li J, Yang Z, et al. A Potent and Protective Human
745 Neutralizing Antibody Against SARS-CoV-2 Variants. Front Immunol. 2021;12:766821. Epub
746 2021/12/31. doi: 10.3389/fimmu.2021.766821. PubMed PMID: 34966387; PubMed Central
747 PMCID: PMC8710476.
748 42. Callaway HM, Zyla D, Larrous F, de Melo GD, Hastie KM, Avalos RD, et al. Structure of
749 the rabies virus glycoprotein trimer bound to a prefusion-specific neutralizing antibody. Sci
750 Adv. 2022;8(24):eabp9151. Epub 2022/06/18. doi: 10.1126/sciadv.abp9151. PubMed PMID:
751 35714192; PubMed Central PMCID: PMC9205594.
752 43. Wang E, Sun H, Wang J, Wang Z, Liu H, Zhang JZH, et al. End-Point Binding Free
753 Energy Calculation with MM/PBSA and MM/GBSA: Strategies and Applications in Drug
754 Design. Chem Rev. 2019;119(16):9478–508. Epub 2019/06/28. doi:
755 10.1021/acs.chemrev.9b00055. PubMed PMID: 31244000.
756 44. Humphrey W, Dalke A, Schulten K. VMD: visual molecular dynamics. J Mol Graph.
757 1996;14(1):33–8, 27–8. Epub 1996/02/01. doi: 10.1016/0263-7855(96)00018-5. PubMed
758 PMID: 8744570.
759 45. REED LJ, MUENCH H. A SIMPLE METHOD OF ESTIMATING FIFTY PER CENT
760 ENDPOINTS12. American Journal of Epidemiology. 1938;27(3):493–7. doi:
761 10.1093/oxfordjournals.aje.a118408.
762 46. Zhang M, Wang H, Foster ER, Nikolov ZL, Fernando SD, King MD. Binding behavior of
763 spike protein and receptor binding domain of the SARS-CoV-2 virus at different
764 environmental conditions. Sci Rep. 2022;12(1):789. Epub 2022/01/19. doi: 10.1038/s41598-
765 021-04673-y. PubMed PMID: 35039570; PubMed Central PMCID: PMC8763896.
766

767

768 **Figure Legends:**

769

770 **Figure 1. Computational insights exploring the cross-reactive SARS-CoV-2 antibodies at**
771 **DENV-2 E protein:** (A) Sequence and structural organization of the DENV-2 E dimer (PDB
772 1OAN). (B) Overview of the computational pipeline. (C) The binding free energy in kcal/mol
773 of selected SARS-CoV-2 antibodies. The most likely complexes were generated using Protein-
774 protein dockings. (D) The interaction map of top three antibodies (CR3022: 6W7Y: violet,
775 S2E12 neutralizing antibody Fab fragment: 7K45: orange and DMAb 2196: 8D8R: magenta)
776 along with the native antibody of DENV-2 E as control (C8:4UTA: green). The residue-wise
777 zoom-out view is shown to highlight the critical residues mainly forming the interactions such
778 as H bonds and SBs. The DENV-2 antibody interactions are shown in green-colored residues
779 and SARS-CoV-2 antibody interactions are highlighted in the pink-colored residues. (E) The
780 matrix of critical residues involved in either establishing either H-bonds or in SBs along with
781 their occurrence. (F) The per-residue decomposition of top three antibodies indicating the
782 thermodynamic contributions of epitope residues. (G) The net binding energy between
783 identified antibodies and DENV-2 E which claims as potential in both cases. (H) The 3D
784 positioning of identified epitope residues at dimer of DENV. The residues which only interact
785 with SARS-CoV-2 antibodies are shown in cyan, the residues interacting with only DENV-2
786 antibody are shown in green color. The residues which are interacting with both DENV-2 E as
787 well as with SARS-CoV-2 RBD are shown in violet color. All the residues are rendered in
788 licorice and atom-wise C: cyan/green/violet, N: blue, O: red and S: yellow.

789

790 **Figure 2: Cross-reactivity and ADE of Dengue virus infection by the SARS-CoV-2 anti-**
791 **RBD antibody CR3022.**

792 (A) Confocal, digital images of DENV-2 (NGC) infected C6/36 cells stained with CR3022
793 along with the controls, 4G2 and Rabishield® (taken from Figure 1 to show the comparison)
794 and the Mean Fluorescence Intensity (MFI). (B) Binding kinetics of (i) CR3022 with SARS-
795 CoV-2 spike protein and (ii) DENV-2 protein E. (C) ADE of DENV-2 infection by different
796 concentrations of CR3022 (2 µg and 4 µg) in K562 cells by flowcytometry. Statistical
797 significance was checked using One-way ANOVA followed by Dunnett's test. Asterisk (*)
798 indicates a statistically significant difference between the control and treatment. P value =
799 0·1234 (ns), 0·0332 (*), 0·0021 (**), 0·0002 (***), <0·0001 (****).
800
801 **Figure 3: ADE of dengue virus infection by the SARS-CoV-2 positive patients' sera in**
802 **K562 cells.**
803 ADE due to convalescent plasma samples collected in the (A)first interval (Samples collected
804 from May 2020- Jan 2021), n=21, (B) second interval (Samples collected from May 2021-June
805 2021), n=17, and (C) third interval (Samples collected from Feb 2022-April 2022), n=10.
806 (D) IgG purified (10 µg) from the five convalescent samples showing the strongest ADE
807 activity was assessed for its potential to enhance DENV infection using Dengue clinical strain
808 (IND-60). The bar graph represents an average percentage increase in DENV positive cells
809 w.r.t. VC for each sample with standard deviation for duplicates. Statistical significance was
810 carried out using One-way ANOVA followed by Dunnett's test in GraphPad Prism 8·4·2.
811 Asterisk (*) indicates that the difference between the virus control and the serum samples is
812 statistically significant. P value = 0·1234 (ns), 0·0332 (*), 0·0021 (**), 0·0002 (***), <0·0001
813 (****). (E) Representative dot plots of patient samples from the first interval (#143, #155),
814 second interval (#96), and third interval (#2, #7). Data was analyzed on FlowJo version 10·8·1.
815

816 **Figure 4: Effect of SARS-CoV-2 on dengue infection in AG129 mice:** (A) Schematic
817 experimental plan showing three animal groups: Mock as G1, adeno-ACE-2 viral vector
818 infection at 5 days prior to day 0 in G2 and G3, SARS-CoV-2 infection at day 2 followed by
819 infection with Dengue virus at day 21 in G2, and dengue virus infection at day 21 in G3. (B)
820 Change in body weight. Two-way ANOVA was used. (C) SARS-CoV-2 Spike antibody
821 response at day 21 (D) DENV2 viral particles were quantified by FFU assay in the serum of
822 infected mice. To compare the two independent groups, the Mann-Whitney U test was applied
823 for the statistical analysis. (E-F) The DENV2 genome was quantified by qRT-PCR from 100mg
824 spleen and liver tissue. Based on the small sample size and comparing the two groups the
825 Student T-test was applied and data are represented as mean ± SEM. *P < 0.05, **P < 0.01, ns
826 = non-significant.
827
828 **Figure 5: Cross-reactivity of antibodies and sera raised against SARS-CoV-2 Spike with**
829 **DENV-2 (NGC) proteins.**
830 (A) Confocal, digital images of DENV-2 (NGC) infected C6/36 cells reacted with 4G2,
831 antibodies and sera raised against SARS-CoV-2 after 48 hpi. Cell nuclei are stained with DAPI
832 while the other antibodies are detected using FITC-labeled respective secondary antibodies.
833 (B) Bar graph showing MFI of 4G2, MSer, 1A9, P1R (normalized w.r.t. the respective
834 secondary antibody controls) with standard deviation. Analysis was performed using ImageJ
835 and statistical significance was carried out using One-way ANOVA followed by Dunnett's test
836 in GraphPad Prism 8·4·2. Asterisk (*) indicates statistically significant difference in MFI w.r.t.
837 Rabishield® (Negative control). P value = 0·1234 (ns), 0·0332 (*), 0·0021 (**), 0·0002 (***),
838 <0·0001 (****). (C) Binding kinetics of C8 (DENV-E protein specific) and 1A9 (SARS-CoV-
839 2 spike specific) antibodies with DENV-2 protein E and SARS-CoV-2 spike protein.
840 Antibodies were loaded onto the sensors and serial dilutions of the proteins were used to study

841 binding kinetics. The binding responses were calculated by subtracting data from reference and
842 fitting globally with a 1:1 binding model using ForteBio's Data Analysis software 10·1. The
843 data was considered validated if $\chi 2 < 0{\cdot}5$.
844
845 **Figure 6: ADE of dengue virus infection by the monoclonal and polyclonal antibodies and**
846 **serum against SARS-CoV-2.**
847 ADE due to (A) anti-spike monoclonal antibodies, M1B (5 µg), 1A9 (5 µg), and different
848 volumes of MM41 (2 µg, 4 µg and 6 µg) and anti-spike polyclonal antibody raised in rabbit,
849 P1R (5 µg), (B) anti-RBD monoclonal antibodies, M4B (5 µg), and different volumes of M5B
850 (2 µg, 4 µg and 6 µg), (C) hamster serum immunized with SARS-CoV-2 spike and negative
851 control (Rabishield®). Statistical significance was calculated using One-way ANOVA
852 followed by Dunnett's test in GraphPad Prism 8·4·2. Asterisk (*) indicates that the difference
853 between the virus control and the serum samples is statistically significant. P value = 0·1234
854 (ns), 0·0332 (*), 0·0021 (**), 0·0002 (***), <0·0001 (****). (D) Representative dot plots. Data
855 was analyzed using FlowJo version 10·8·1.
856
857
858
859
860

Figure 1

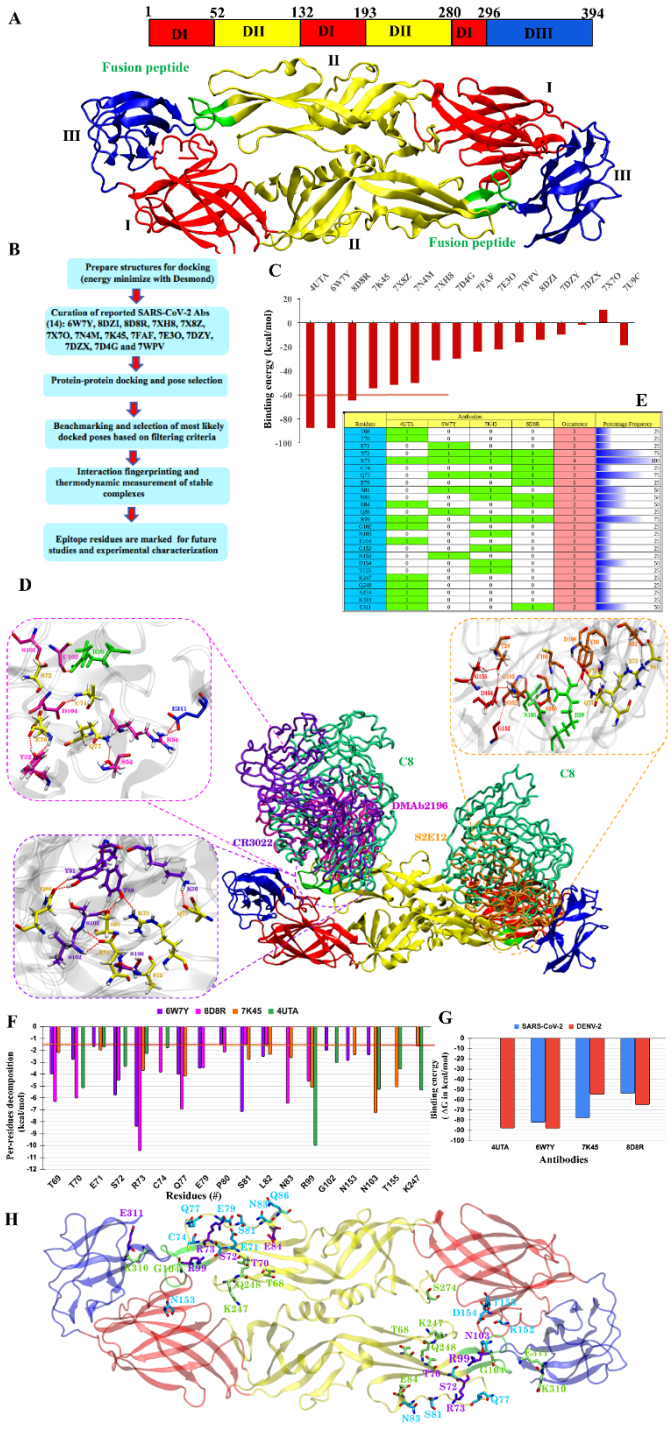
A
1
52
132
193
280
296
394
DI
DII
DI
DII
DI
DIII
Fusion peptide
II
I
III
III
I
II
Fusion peptide
B
Prepare structures for docking (energy minimize with Desmond)
Curation of reported SARS-CoV-2 Abs (14): 6W7Y, 8DZI, 8D8R, 7XH8, 7X8Z, 7X7O, 7N4M, 7K45, 7FAF, 7E3O, 7DZY, 7DZX, 7D4G and 7WPV
Protein-protein docking and pose selection
Benchmarking and selection of most likely docked poses based on filtering criteria
Interaction fingerprinting and thermodynamic measurement of stable complexes
Epitope residues are marked for future studies and experimental characterization
C
Binding energy (kcal/mol)
E
D
C8
DMAb2196
S2E12
CR3022
F
6W7Y
8D8R
7K45
4UTA
Per-residues decomposition (kcal/mol)
Residues (#)
G
SARS-CoV-2
DENV-2
Binding energy (ΔG in kcal/mol)
Antibodies
H

Figure 2

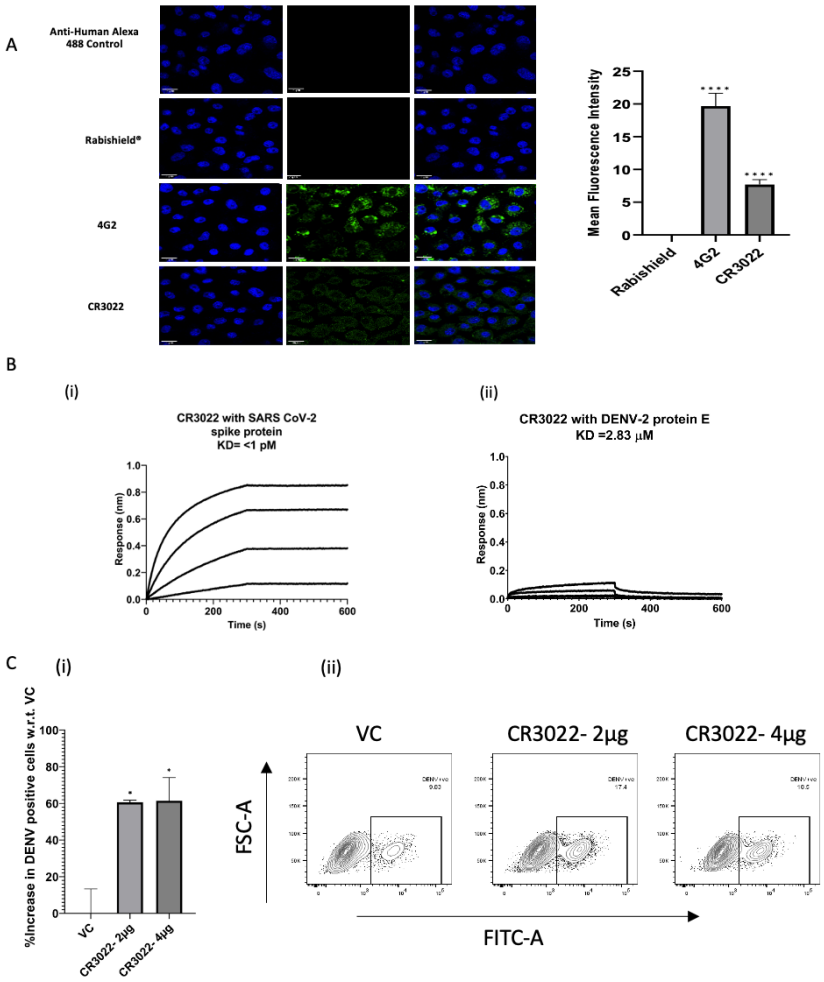
A
Anti-Human Alexa 488 Control
Rabishield®
4G2
CR3022
Mean Fluorescence Intensity
Rabishield
4G2
CR3022
B
(i)
CR3022 with SARS CoV-2 spike protein KD= <1 pM
Response (nm)
Time (s)
(ii)
CR3022 with DENV-2 protein E KD =2.83 µM
Response (nm)
Time (s)
C
(i)
%Increase in DENV positive cells w.r.t. VC
VC
CR3022- 2µg
CR3022- 4µg
(ii)
VC
CR3022- 2µg
CR3022- 4µg
FSC-A
FITC-A

Figure 3

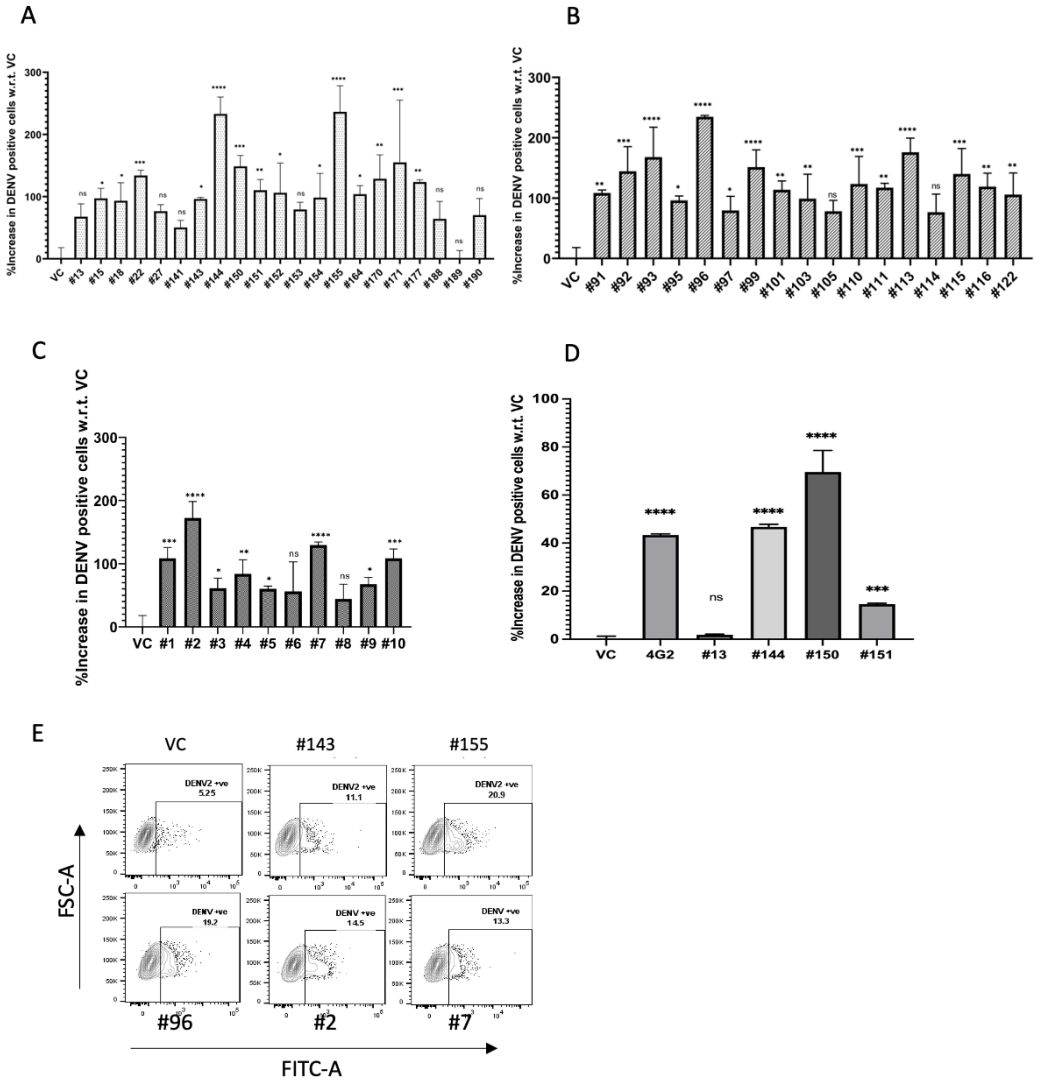
A
%Increase in DENV positive cells w.r.t. VC
VC #13 #15 #18 #22 #27 #141 #143 #144 #150 #151 #152 #153 #154 #155 #164 #170 #171 #177 #188 #189 #190
B
%Increase in DENV positive cells w.r.t. VC
VC #91 #92 #93 #95 #96 #97 #99 #101 #103 #105 #110 #111 #113 #114 #115 #116 #122
C
%Increase in DENV positive cells w.r.t. VC
VC #1 #2 #3 #4 #5 #6 #7 #8 #9 #10
D
%Increase in DENV positive cells w.r.t. VC
VC 4G2 #13 #144 #150 #151
E
VC
#143
#155
DENV2 +ve 5.25
DENV2 +ve 11.1
DENV2 +ve 20.9
DENV +ve 19.2
DENV +ve 14.5
DENV +ve 13.3
#96
#2
#7
FSC-A
FITC-A

Figure 4

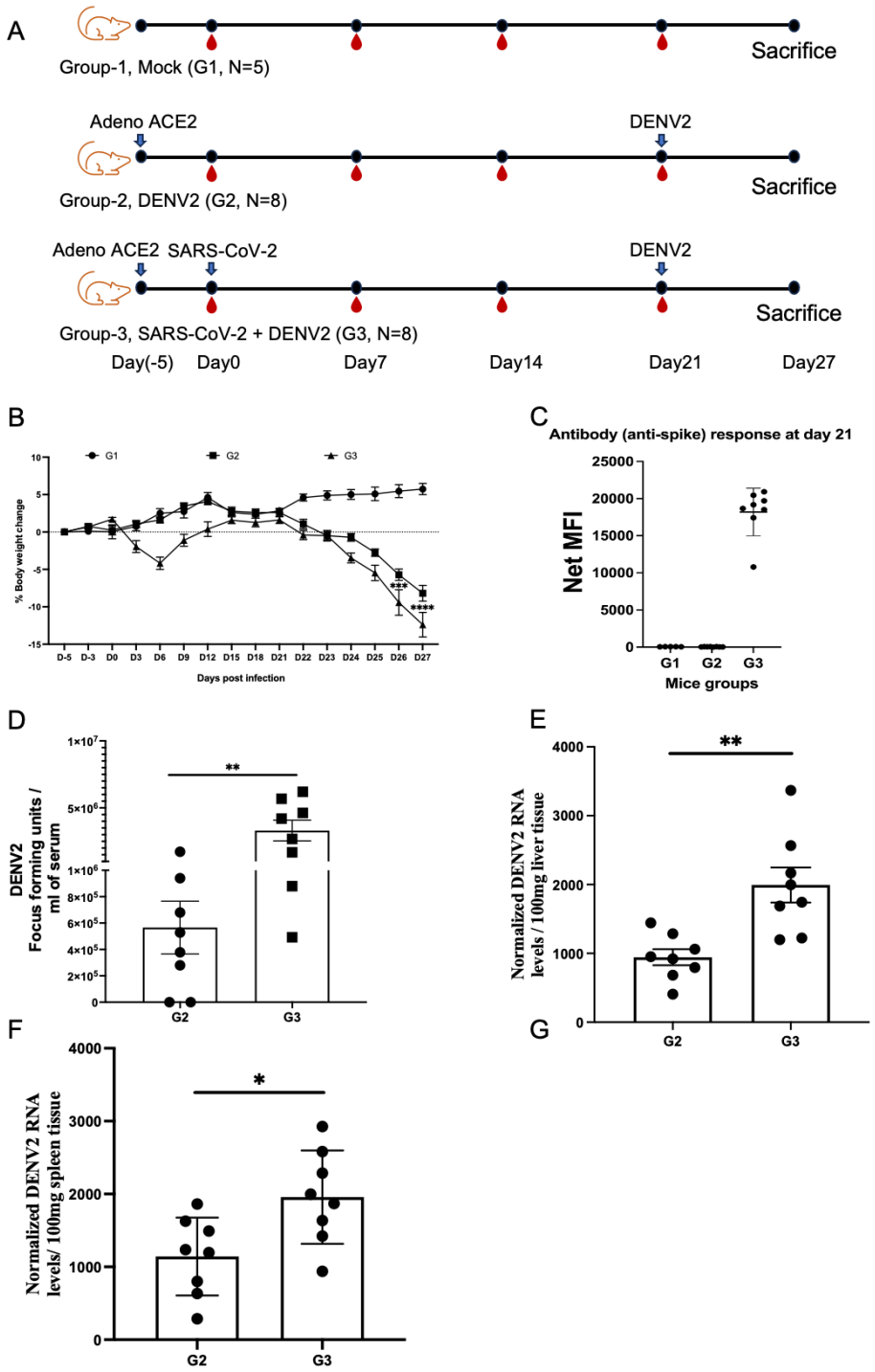
A
Group-1, Mock (G1, N=5)
Sacrifice
Adeno ACE2
DENV2
Group-2, DENV2 (G2, N=8)
Sacrifice
Adeno ACE2 SARS-CoV-2
DENV2
Group-3, SARS-CoV-2 + DENV2 (G3, N=8)
Sacrifice
Day(-5) Day0 Day7 Day14 Day21 Day27
B
G1
G2
G3
% Body weight change
Days post infection
C
Antibody (anti-spike) response at day 21
Net MFI
Mice groups
D
DENV2 Focus forming units / ml of serum
E
Normalized DENV2 RNA levels / 100mg liver tissue
F
Normalized DENV2 RNA levels/ 100mg spleen tissue
G

Figure 5

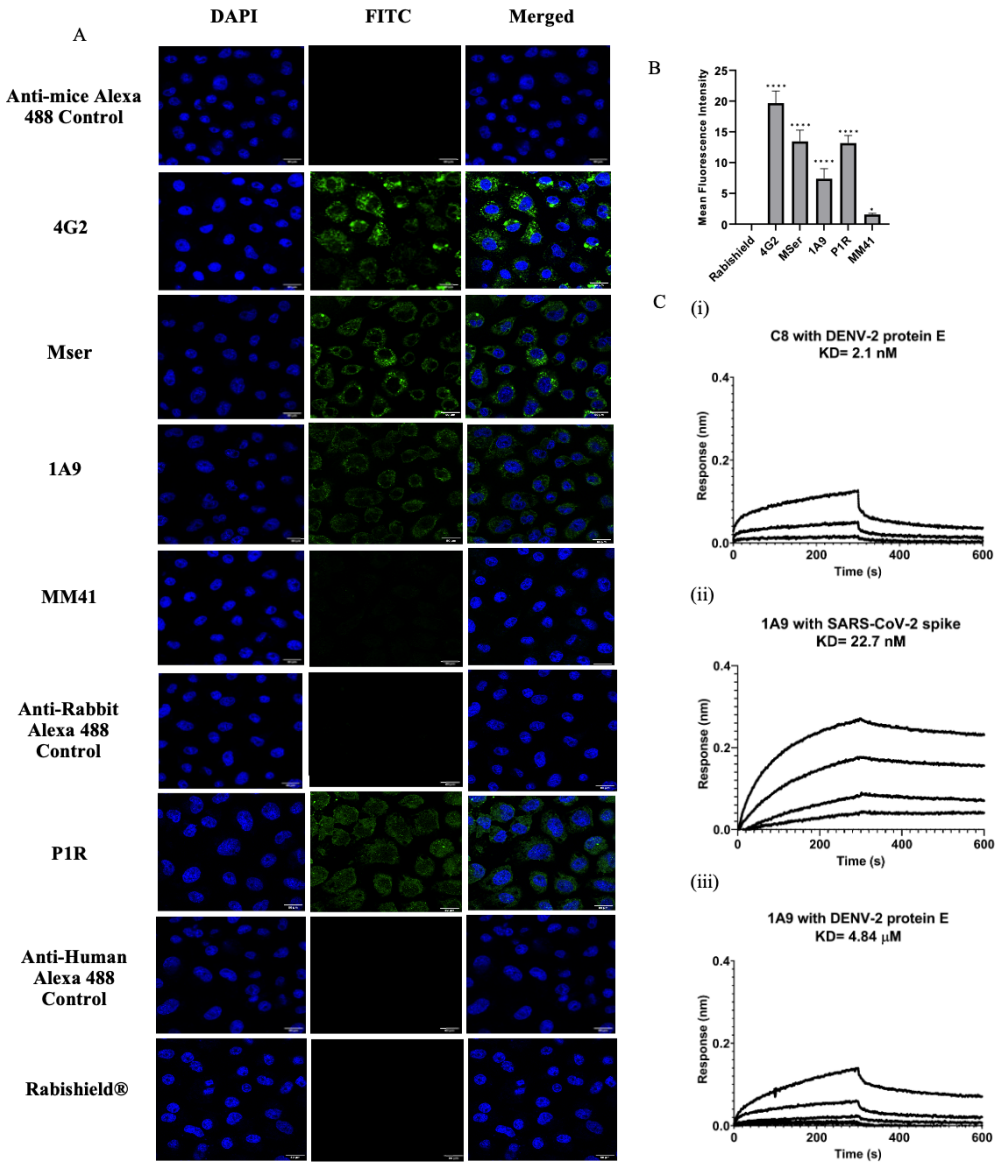
A
DAPI
FITC
Merged
Anti-mice Alexa 488 Control
4G2
Mser
1A9
MM41
Anti-Rabbit Alexa 488 Control
P1R
Anti-Human Alexa 488 Control
Rabishield®
B
Mean Fluorescence Intensity
Rabishield
4G2
MSer
1A9
P1R
MM41
C
(i)
C8 with DENV-2 protein E
KD= 2.1 nM
Response (nm)
Time (s)
(ii)
1A9 with SARS-CoV-2 spike
KD= 22.7 nM
Response (nm)
Time (s)
(iii)
1A9 with DENV-2 protein E
KD= 4.84 µM
Response (nm)
Time (s)

Figure 6

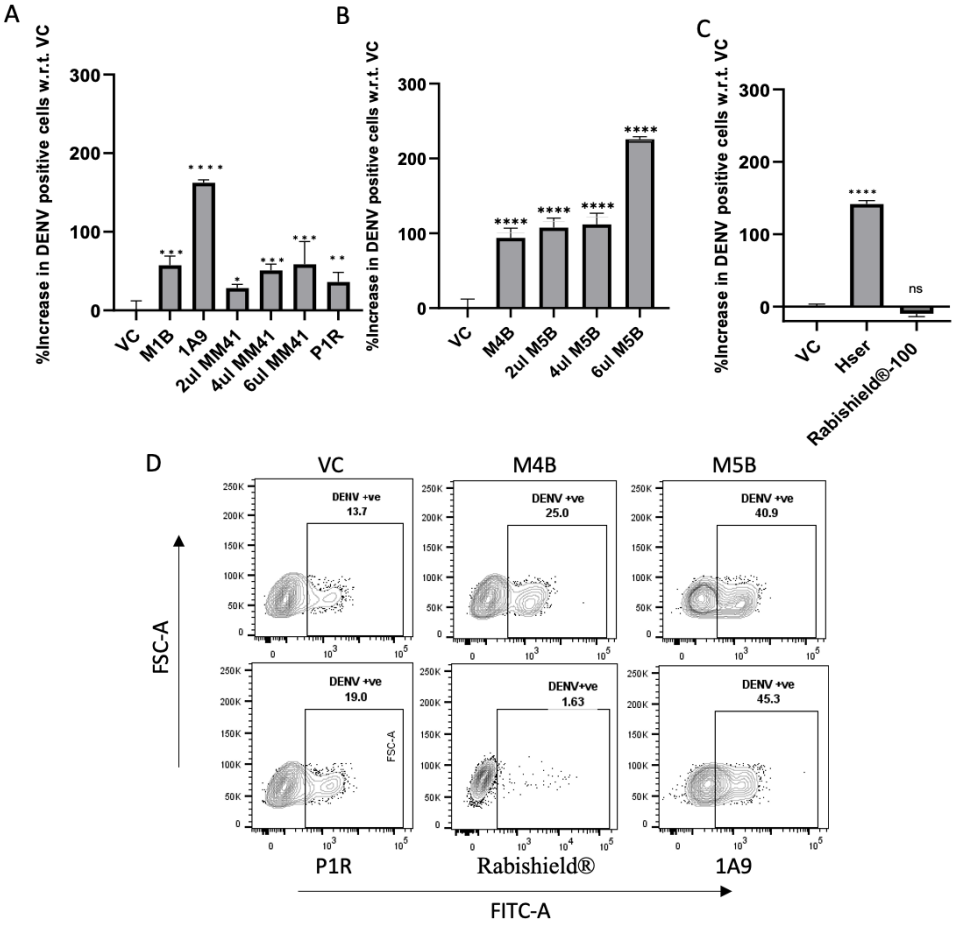
A
%Increase in DENV positive cells w.r.t. VC
300
200
100
0
VC
M1B
1A9
2ul MM41
4ul MM41
6ul MM41
P1R
B
%Increase in DENV positive cells w.r.t. VC
VC
M4B
2ul M5B
4ul M5B
6ul M5B
C
%Increase in DENV positive cells w.r.t. VC
VC
Hser
Rabishield®-100
ns
D
VC
M4B
M5B
DENV +ve 13.7
DENV +ve 25.0
DENV +ve 40.9
DENV +ve 19.0
DENV+ve 1.63
DENV +ve 45.3
FSC-A
P1R
Rabishield®
1A9
FITC-A

Figure 1

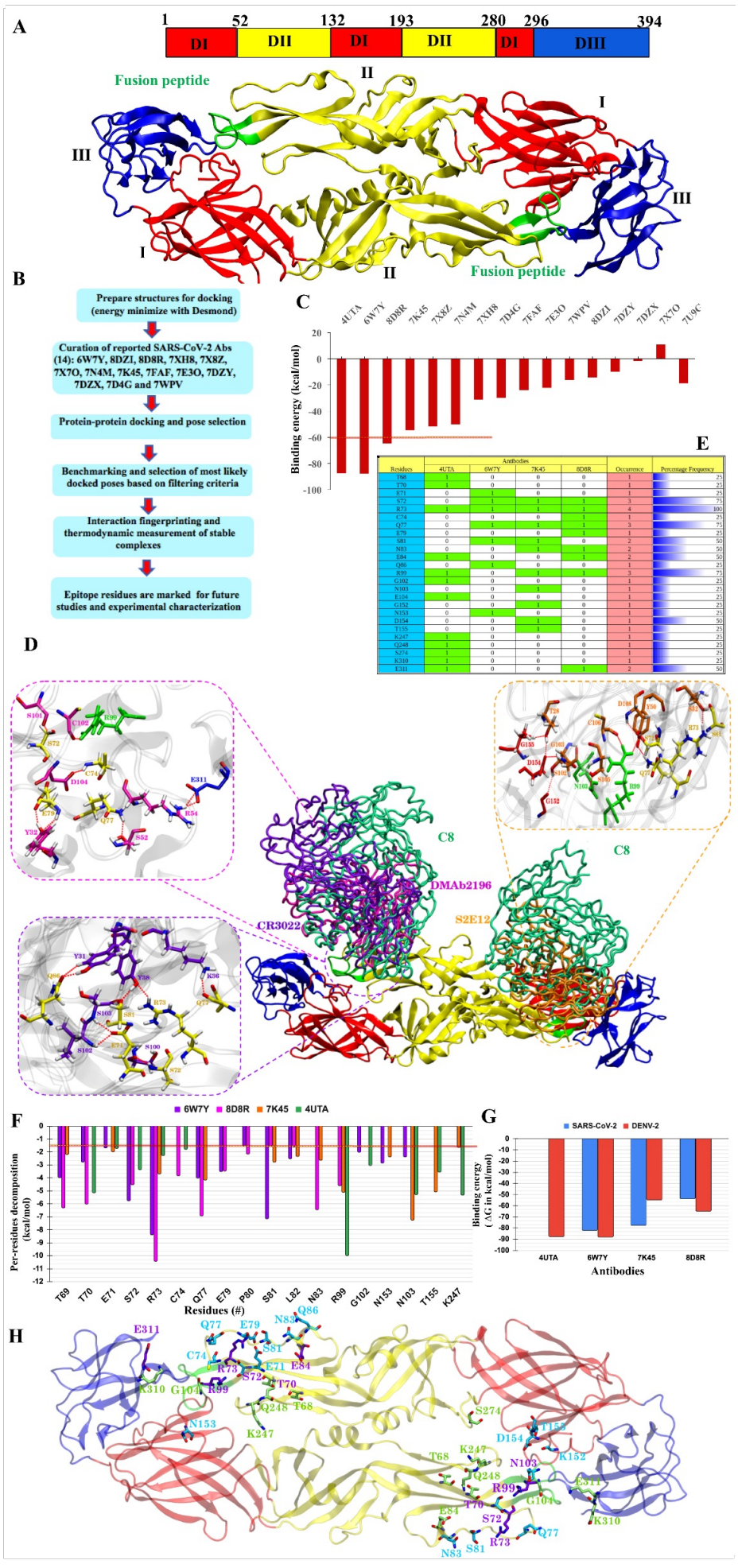

Residues	Antibodies				Occurrence	Percentage Frequency
	4UTA	6W7Y	7K45	8D8R		
T68	1	0	0	0	1	25
T70	1	0	0	0	1	25
E71	0	1	0	0	1	25
S72	0	1	1	1	3	75
R73	1	1	1	1	4	100
C74	0	0	0	1	1	25
Q77	0	1	1	1	3	75
E79	0	0	0	1	1	25
S81	0	1	1	0	2	50
N83	0	0	1	1	2	50
E84	1	0	0	1	2	50
Q86	0	1	0	0	1	25
R99	1	0	1	1	3	75
G102	1	0	0	0	1	25
N103	0	0	1	0	1	25
E104	1	0	0	0	1	25
G152	0	0	1	0	1	25
N153	0	1	0	0	1	25
D154	0	0	1	0	1	50
T155	0	0	1	0	1	25
K247	1	0	0	0	1	25
Q248	1	0	0	0	1	25
S274	1	0	0	0	1	25
K310	1	0	0	0	1	25
E311	1	0	0	1	2	50

Figure 2

A

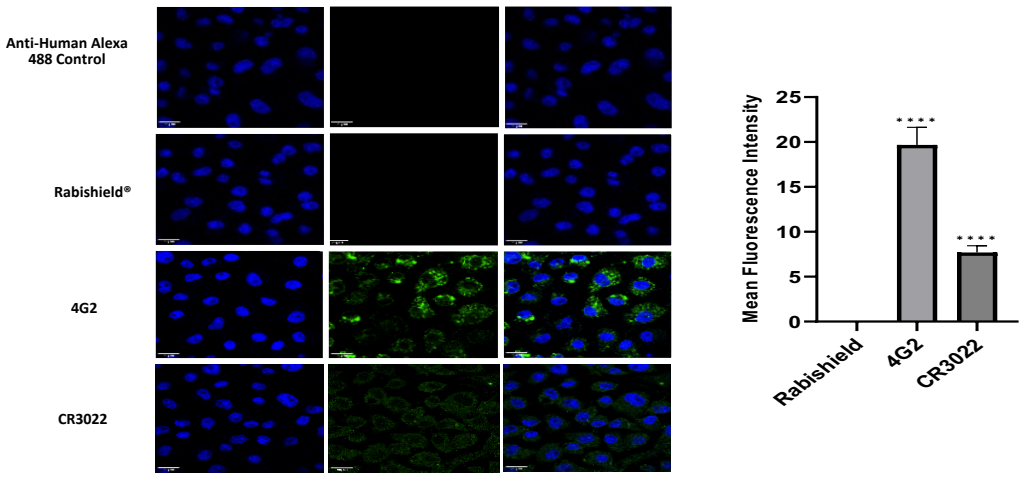
Anti-Human Alexa 488 Control
Rabishield®
4G2
CR3022
Mean Fluorescence Intensity
25
20
15
10
5
0
Rabishield
4G2
CR3022

B

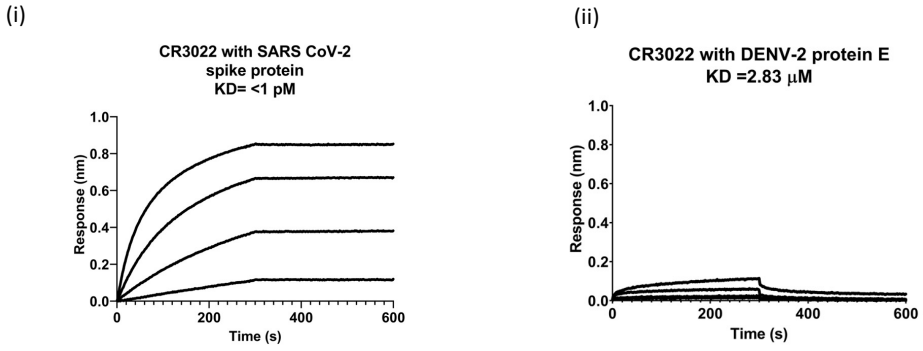
(i)
CR3022 with SARS CoV-2 spike protein
KD= <1 pM
Response (nm)
Time (s)
(ii)
CR3022 with DENV-2 protein E
KD =2.83 μM
Response (nm)
Time (s)

C

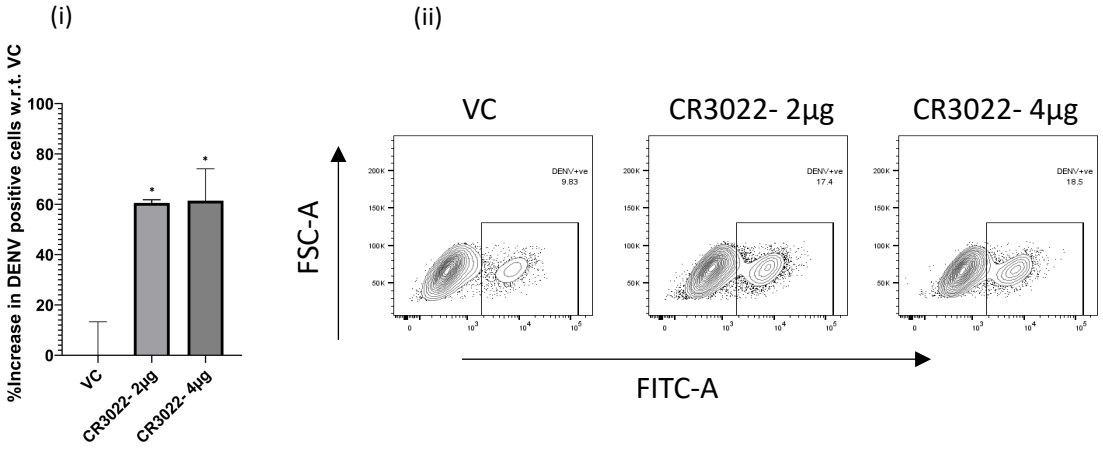
(i)
%Increase in DENV positive cells w.r.t. VC
VC
CR3022- 2μg
CR3022- 4μg
(ii)
VC
CR3022- 2μg
CR3022- 4μg
FSC-A
FITC-A

Figure 3

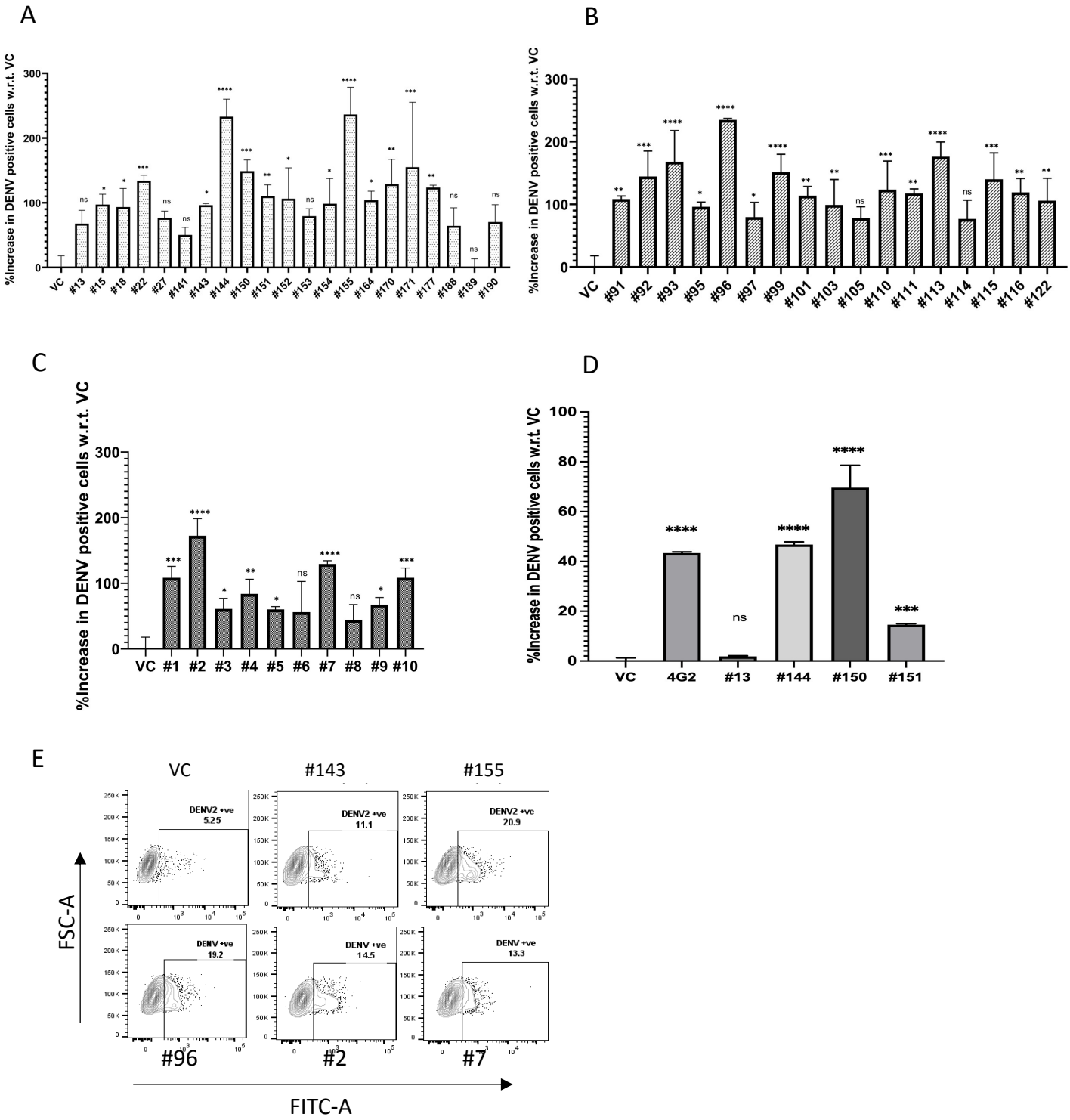
A
%Increase in DENV positive cells w.r.t. VC
VC #13 #15 #18 #22 #27 #141 #143 #144 #150 #151 #152 #153 #154 #155 #164 #170 #171 #177 #188 #189 #190
B
%Increase in DENV positive cells w.r.t. VC
VC #91 #92 #93 #95 #96 #97 #99 #101 #103 #105 #110 #111 #113 #114 #115 #116 #122
C
%Increase in DENV positive cells w.r.t. VC
VC #1 #2 #3 #4 #5 #6 #7 #8 #9 #10
D
%Increase in DENV positive cells w.r.t. VC
VC 4G2 #13 #144 #150 #151
E
VC
#143
#155
DENV2 +ve 5.25
DENV2 +ve 11.1
DENV2 +ve 20.9
DENV +ve 19.2
DENV +ve 14.5
DENV +ve 13.3
#96
#2
#7
FSC-A
FITC-A

Figure 4

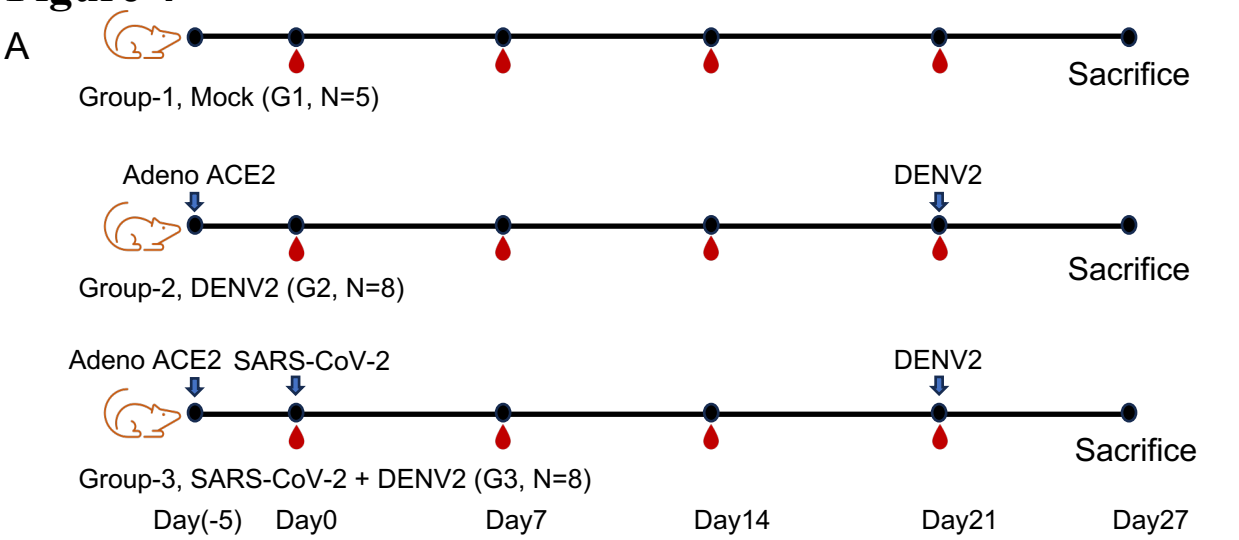
A
Group-1, Mock (G1, N=5)
Sacrifice
Adeno ACE2
DENV2
Group-2, DENV2 (G2, N=8)
Sacrifice
Adeno ACE2
SARS-CoV-2
DENV2
Group-3, SARS-CoV-2 + DENV2 (G3, N=8)
Sacrifice
Day(-5)
Day0
Day7
Day14
Day21
Day27

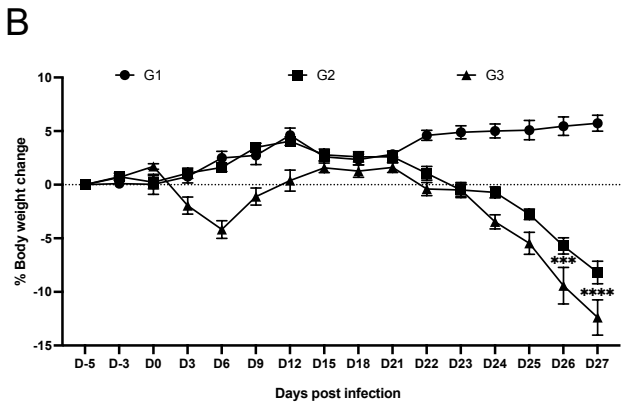
B
G1
G2
G3
% Body weight change
10
5
0
-5
-10
-15
***
****
D-5
D-3
D0
D3
D6
D9
D12
D15
D18
D21
D22
D23
D24
D25
D26
D27
Days post infection

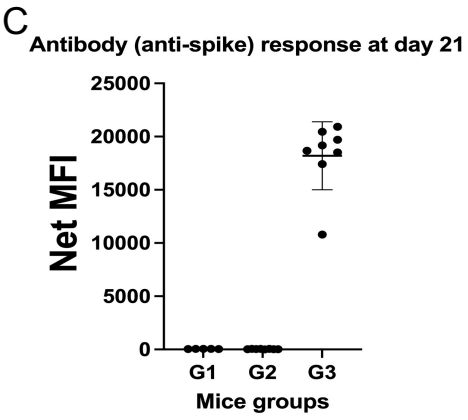
C
Antibody (anti-spike) response at day 21
Net MFI
25000
20000
15000
10000
5000
0
G1
G2
G3
Mice groups

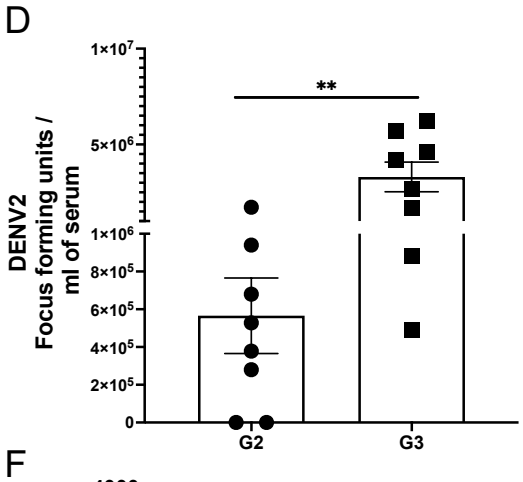
D
DENV2
Focus forming units / ml of serum
1×10^7
5×10^6
1×10^6
8×10^5
6×10^5
4×10^5
2×10^5
0
**
G2
G3

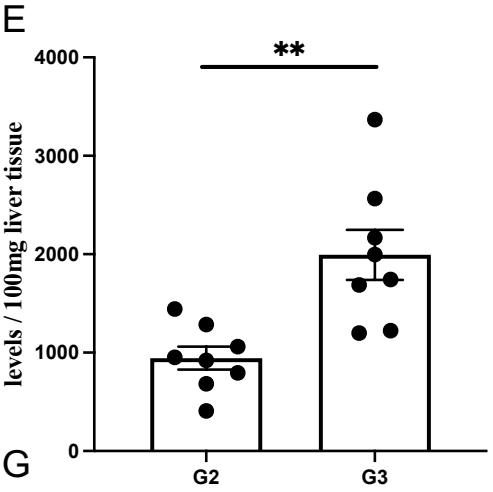
E
Normalized DENV2 RNA levels / 100mg liver tissue
4000
3000
2000
1000
0
**
G2
G3

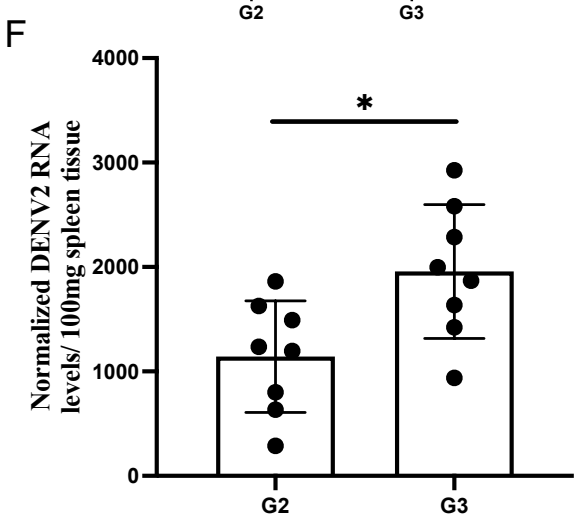
F
Normalized DENV2 RNA levels/ 100mg spleen tissue
4000
3000
2000
1000
0
*
G2
G3

G

Figure 5

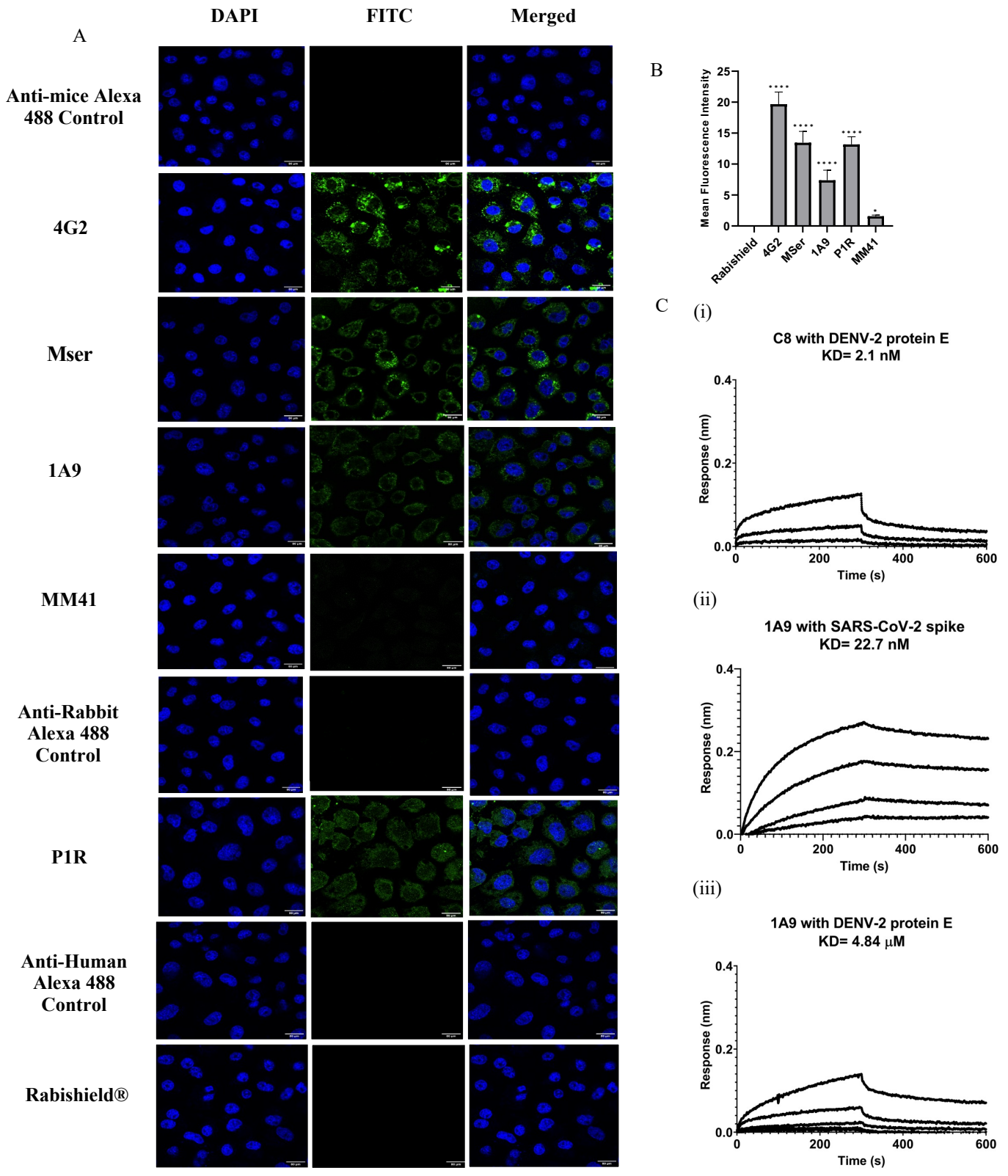
A
DAPI
FITC
Merged
Anti-mice Alexa 488 Control
4G2
Mser
1A9
MM41
Anti-Rabbit Alexa 488 Control
P1R
Anti-Human Alexa 488 Control
Rabishield®
B
Mean Fluorescence Intensity
25
20
15
10
5
0
Rabishield
4G2
MSer
1A9
P1R
MM41
C
(i)
C8 with DENV-2 protein E
KD= 2.1 nM
Response (nm)
0.4
0.2
0.0
0
200
400
600
Time (s)
(ii)
1A9 with SARS-CoV-2 spike
KD= 22.7 nM
Response (nm)
0.4
0.2
0.0
0
200
400
600
Time (s)
(iii)
1A9 with DENV-2 protein E
KD= 4.84 μM
Response (nm)
0.4
0.2
0.0
0
200
400
600
Time (s)

Figure 6

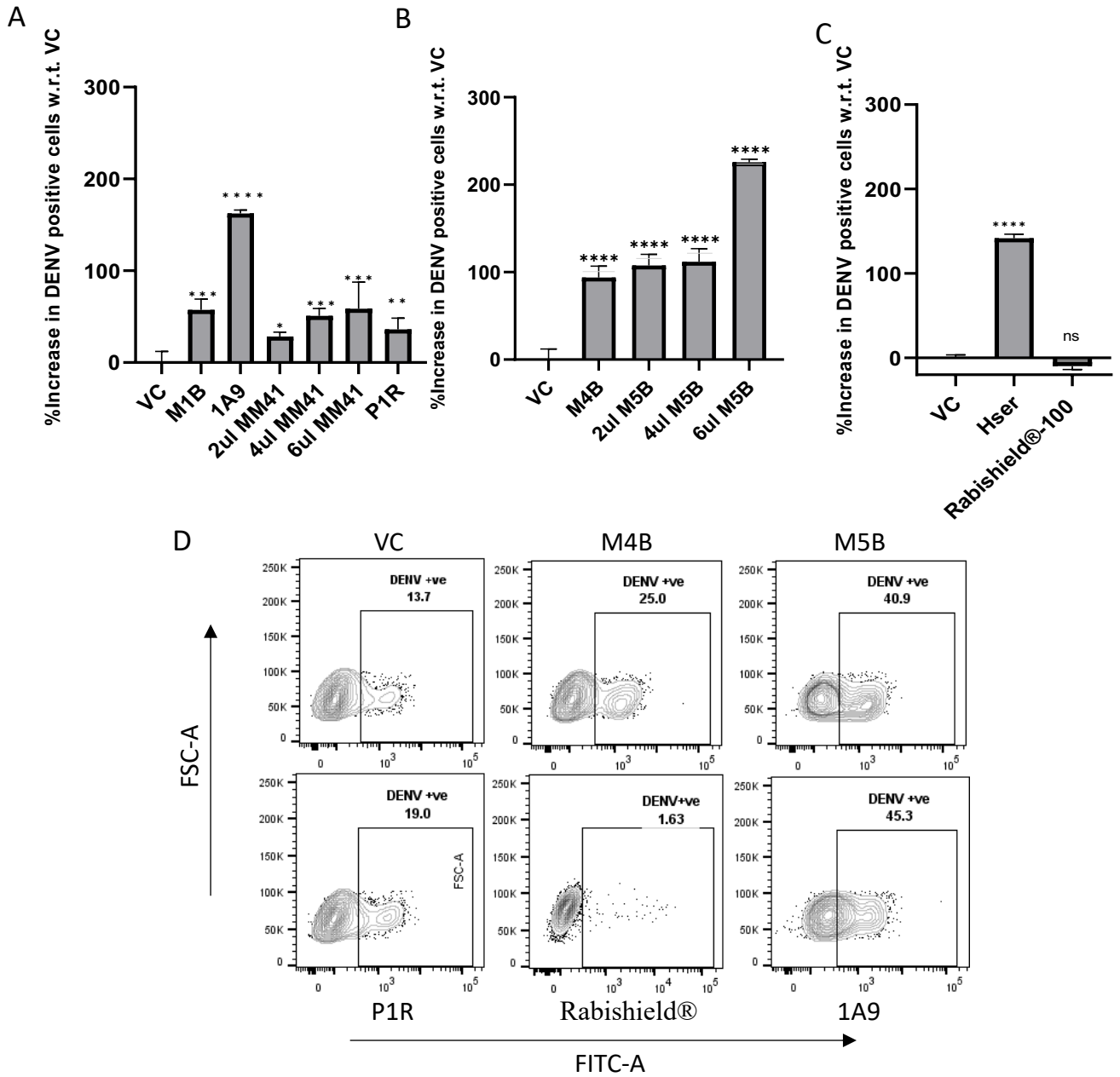
A
%Increase in DENV positive cells w.r.t. VC
300
200
100
0
VC
M1B
1A9
2ul MM41
4ul MM41
6ul MM41
P1R
B
%Increase in DENV positive cells w.r.t. VC
VC
M4B
2ul M5B
4ul M5B
6ul M5B
C
%Increase in DENV positive cells w.r.t. VC
ns
VC
Hser
Rabishield®-100
D
VC
M4B
M5B
DENV +ve 13.7
DENV +ve 25.0
DENV +ve 40.9
DENV +ve 19.0
DENV+ve 1.63
DENV +ve 45.3
FSC-A
P1R
Rabishield®
1A9
FITC-A